Chapter 6

Development of multi-targetable chalcone derivatives bearing *N*-aryl piperazine moiety

Chapter 6

Development of multi-targetable chalcone derivatives bearing *N*-aryl piperazine moiety

6.1 Design strategy

The multi-targetable chalcone derivatives bearing N-aryl piperazine were designed with the strategy depicted in **Figure 6.1**. As per the well-established cholinergic hypothesis, targeting cholinesterase enzymes, i.e., AChE and BuChE, is promising approach for developing therapeutics for the treatment of AD. The design of BACE-1 and Aβ aggregation inhibitors is another crucial approach to the reported hypothesis (170). The strategy of scaffold hopping guided novel multi-target-directed ligands (MTDLs) has been employed to target both cholinesterase and $A\beta_{1-42}$ hypotheses, simultaneously. To develop the multi-targetable ligands, hybrid molecules consisting of distinct pharmacophores that act upon targets were designed. The novel scaffold was constructed through the modification of the structural features of the existing/reported potential anti-AD agents acting on the respective targets. Precisely, the molecules were derived by amalgamating structural features from the reported potent cholinesterase inhibitors (AChE & BuChE), BACE-1, and Aβ aggregation. The chalcone moiety, a component of many natural flavonoids and iso-flavonoids, has been established as a privileged scaffold in medicinal chemistry due to its comprehensive range of biological activities. It is the preferred scaffold for its therapeutic potential in AD due to several advantages, i.e., small molecular size, cost-effective synthesis, and flexibility for modifications to modulate biological activity and has also been explored against different targets of AD (171). A novel class of fluoro-substituted tris-chalcones derivatives has been reported by Burmaoglu S. *et al.* for the inhibitory potential on the carbonic anhydrase, acetylcholinesterase, butyrylcholinesterase, and α-glycosidase. Interestingly, it produced potent inhibitory activities, 1.09 - 6.84 nM and 8.30 - 32.30 nM for the AChE and BuChE, respectively (172). Zhiyuan Zhu and co-workers reported 2, 2', 4"-trihydroxychalcone

(TDC) from *Glycyrrhiza glabra* as a potent BACE-1 inhibitor. The *in vivo* results showed an improvement in memory impairment in mice, highlighting the importance of the scaffold (173). The well-known natural product curcumin, which is structurally close to the chalcone, has been reported to inhibit the formation of Aβ oligomers and fibrils and reduce the Aβ *in vivo* (174). Presently, Curcumin has entered in Phase II clinical trial for the treatment of AD (NCT00099710). The piperazine moiety has also been widely explored for its anti-AD potential. Piperazine-containing compounds (**1, 2 & VK-28**) showed strong neuronal protection and anti-neuroinflammatory activity, which contributed to anti-AD activity (175, 176, 177). Furthermore, the structural features of established DNZ and its structural analogs with potent anti-cholinesterase activity have also been taken into consideration. Compounds **3** and **4** showed potent inhibition of AChE with IC_{50} of 0.8 and 0.41 nM, respectively, and have also been included in the design (178, 179).

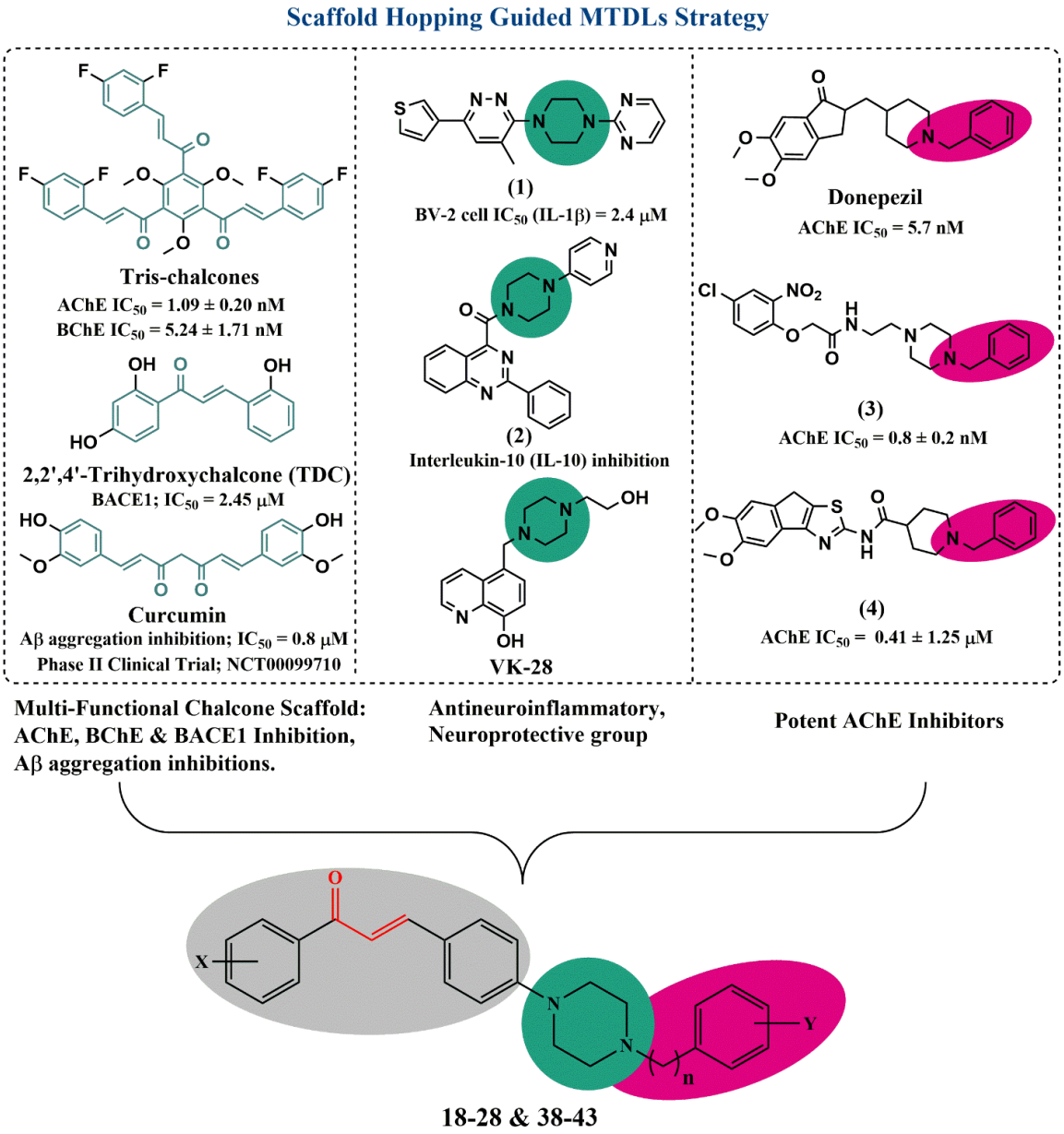

Figure 6.1. Strategy for design of multi-target-directed ligand for AD.

6.2 Experimental procedures

6.2.1 Chemistry

All the chemicals and reagents used in the synthesis were purchased from Alfa Acer, Avra Synthesis, Sigma Aldrich, TCI Chemicals and used without further purification unless otherwise mentioned. The progress of the reaction was monitored by using thin-layer chromatography (TLC) plates on precoated silica gel 60 F254 (Merck KGaA). Spots on TLC plates were visualized under ultraviolet light or iodine vapors as needed. The

automated melting point system (Barnstead Electrothermal, UK) was used to measure the melting points of all the synthesized compounds. The proton (^{1}H) and carbon (^{13}C) NMR spectra were acquired on Bruker Advance, 500 MHz & 125 MHz spectrometers, respectively with tetramethylsilane (TMS) as the internal standard. $CDCl_3$ and DMSO–d_6 were used as NMR solvents at room temperature. The chemical shifts are presented in terms of ppm (d values) with respect to an internal TMS. The % purity of the compounds was determined on high-performance liquid chromatography (Shimadzu, USA) using CH_3CN/H_2O/TFA (95:5:0.1%) as the mobile phase in the C_{18} column. The data is incorporated in the supporting information in section (C) a**s** figures **S13, S14** and **S15**. The mass spectra of compounds were obtained with a SCIEX. X500R QTOF, US, instrument equipped with an APCI and ESI multimode ionization source.

6.2.1.1 General procedure for the synthesis of compounds 8-9 & 31

To the mixture of 4-Fluorobenzaldehyde (**5**) (1.0 equiv) and anhydrous potassium carbonate (K_2CO_3) (2.0 equiv) in dimethylformamide (DMF) 5 ml, appropriately substituted piperazine (**6-7**/**30**) (1.0 equiv) was added. The mixture, in a round-bottom (R.B) flask with provision of a magnetic stirrer, was refluxed for 12h at 100°C. The progress of the reaction was monitored by TLC with the mobile phase, ethyl acetate, and hexane (4:6). After completion of the reaction, the mixture was poured into ice water. The solid formed was filtered and washed with water and petroleum ether to achieve pure product (**8-9 & 31)** in good yields.

4-(4-phenylpiperazine-1-yl)benzaldehyde **(8):** Pale yellow solid, yield: 88%, M.P.: 141-143 °C. ^{1}H NMR (500 MHz, $CDCl_3$): δ 9.82 (s, 1H, aldehyde CHO), 7.81 (d, J = 8.9 Hz, 2H, benzaldehyde C_2,C_6), 7.05 – 6.95 (m, 5H, phenylpiperazine), 6.90 (d, J = 9.0 Hz, 2H, benzaldehyde C_3,C_5), 3.63 – 3.55 (m, 4H, piperazine C_2,C_6), 3.30 – 3.20 (m, 4H, piperazine C_3,C_5). ^{13}C NMR (125 MHz, $CDCl_3$) δ 190.46 (aldehyde C=O), 154.98

(phenylpiperazine C_1), 144.65 (benzaldehyde C_4), 131.89 (benzaldehyde C_6), 130.11 (benzaldehyde C_2), 129.23 (phenylpiperazine C_5), 128.54 (phenylpiperazine C_3), 127.39 (benzaldehyde C_1), 118.70 (phenylpiperazine C_4), 115.09 (phenylpiperazine C_6), 114.59 (phenylpiperazine C_2), 114.57 (benzaldehyde C_5), 113.75 (benzaldehyde C_3), 55.60 (piperazine C_2), 50.64 (piperazine C_6), 48.16 (piperazine C_3), 47.41 (piperazine C_5). MS (EI+): *m/z* calculated for $C_{17}H_{18}N_2O$: 266.34, found – 267.4311 (M+1).

***4-(4-(4-methoxyphenyl)piperazin-1-yl)benzaldehyde* (9):** Pale yellow solid, yield: 85%, M.P.: 138-140°C. ^{1} H NMR (500 MHz, $CDCl_3$): δ 9.87 (s, 1H, aldehyde CHO), 7.79 (d, *J* = 8.9 Hz, 2H, benzaldehyde C_2, C_6), 7.49 (d, *J* = 8.2 Hz, 2H, benzaldehyde C_3, C_5), 7.01 (d, *J* = 8.5 Hz, 2H, 4-methoxyphenyl C_2, C_6) 6.68 (d, *J* = 8.1 Hz, 2H, 4-methoxyphenyl C_3, C_5), 3.84 – 3.78 (s, 3H, OCH_3), 3.64 – 3.55 (m, 4H, piperazine C_2,C_6), 3.55 – 3.47 (m, 4H, piperazine C_3,C_5). ^{13}C NMR (125 MHz, $CDCl_3$) δ 191.99 (aldehyde CHO), 156.20 (), 152.81 (4-methoxyphenyl C_4), 143.34 (4-methoxyphenyl C_1), 135.59 (benzaldehyde C_4), 133.12 (benzaldehyde C_2, C_6), 128.59 (benzaldehyde C_1), 116.43 (4-methoxyphenyl C_2, C_6),115.95 (4-methoxyphenyl C_3, C_5), 111.69 (benzaldehyde C_3, C_5), 56.04 (OCH_3), 55.21 (piperazine C_2), 50.42 (piperazine C_6), 48.51 (piperazine C_3), 46.35 (piperazine C_5). MS (EI+): *m/z* calculated for $C_{18}H_{20}N_2O_2$: 296.37, found – 297.4322 (M+1).

***4-(4-benzylpiperazin-1-yl)benzaldehyde* (31):** Dark yellow solid, yield: 78%, M.P.: 160-162°C. ^{1} H NMR (500 MHz, $CDCl_3$): δ 9.86 (s, 1H, aldehyde CHO), 7.47 (d, *J* = 8.6 Hz, 2H, benzyl C_3, C_5), 7.36 – 7.24 (m, 4H, benzyl C_2, C_6, benzaldehyde C_2, C_6), 7.22 (s, 1H, benzyl C_4), 6.96 (d, *J* = 8.1 Hz, 2H, benzaldehyde C_3, C_5), 3.73 (s, 2H, benzyl CH_2), 3.67 – 3.56 (m, 4H, piperazine C_2,C_6), 2.93 – 2.85 (m, 4H, piperazine C_3,C_5). ^{13}C NMR (125 MHz, $CDCl_3$) δ 191.99 (aldehyde CHO), 156.20 (benzaldehyde C_4), 138.23 (benzyl C_1), 133.12 (benzaldehyde C_2, C_6), 128.58 (benzyl C_2, C_6), 128.39 (benzyl C_3, C_5), 127.49

(benzyl C_4), 126.55 (benzaldehyde C_1), 111.79 (benzaldehyde C_3, C_5), 63.66 (benzyl CH_2), 56.46 (piperazine C_2), 50.37 (piperazine C_6), 48.72 (piperazine C_3), 47.84 (piperazine C_5). MS (EI+): *m/z* calculated for $C_{18}H_{20}N_2O$: 280.37, found – 281.4815 (M+1).

6.2.1.2 General procedure for the synthesis of compounds 18-28; 38-43

A solution of compound (**6-7**/**30**) (1.5 equiv) and appropriate substituted acetophenone (**10-17**/**32-37**) (1.0 equiv) in ethanol was cooled at 0°C. An aqueous 2.5 M NaOH solution was added dropwise (1 ml). The reaction mixture was stirred at room temperature for 8−12 h. After adding cold water and subsequent neutralization with acetic acid, the precipitate obtained was filtered and washed with cold ethanol. The crude product was purified using column chromatography with silica gel (60-120 mesh) and solvents (ethyl acetate/n-hexane) to afford desired derivatives **18-28; 38-43.**

(E)-3-(4-(4-phenylpiperazin-1-yl)phenyl)-1-(p-tolyl)prop-2-en-1-one **(18)*:*** Bright yellow solid, Yield: 80%, M.P 138-136 °C. ^{1}H NMR (500 MHz, $CDCl_3$): δ 7.95 (d, *J* = 8.2 Hz, 2H, tolyl C_2,C_6), 7.80 (d, *J* = 15.6 Hz, 1H, chalcone CH), 7.61 (d, *J* = 8.9 Hz, 2H, phenylpiperazine C_3,C_5), 7.42 (d, *J* = 15.6 Hz, 1H, chalcone CH), 7.33 (t, *J* = 8.0 Hz, 4H, tolyl C_3,C_5, phenyl C_3,C_5), 7.00 (dd, *J* = 13.7, 8.2 Hz, 4H, phenylpiperazine C_2,C_6, phenyl C_2, C_6), 6.93 (t, *J* = 7.3 Hz, 1H, phenyl C_4), 3.56 – 3.47 (m, 4H, piperazine C_2,C_6), 3.44 – 3.35 (m, 4H, piperazine C_3,C_5), 2.46 (s, 3H *p*-methyl). ^{13}C NMR (125 MHz, $CDCl_3$) δ 190.16 (C=O), 152.54 (phenyl C_1), 151.06 (tolyl C_4), 144.63 (chalcone CH), 130.11 (tolyl C_1, phenylpiperazine C_1), 129.26 (tolyl C_2,C_6), 129.23 (tolyl C_3,C_5), 128.54 (phenylpiperazine C_3,C_5), 120.29 (phenyl C_4), 118.69 (chalcone CH), 116.40 (phenyl C_2, C_6), 115.07 (phenylpiperazine C_2,C_6), 49.20 (piperazine C_2, C_6), 48.03 (piperazine C_3, C_5), 21.65 (methyl). MS (EI+): *m/z* calculated for $C_{26}H_{26}N_2O$: 382.20, found – 383.2117 (M+1).

(E)-1-(4-bromophenyl)-3-(4-(4-phenylpiperazin-1-yl)phenyl)prop-2-en-1-one **(19)*:*** Yellow solid, yield: 75%, M.P.: 133-135°C. ^{1}H NMR (500 MHz, $CDCl_3$): δ 8.76 (s, 1H, 4-bromophenyl C_5), 8.35 (d, *J* = 8.3 Hz, 1H, 4-bromophenyl C_2), 8.27 (d, *J* = 7.9 Hz, 1H, 4-bromophenyl C_6), 7.80 (d, *J* = 12.0 Hz, 1H, chalcone CH), 7.63 (t, *J* = 6.1 Hz, 1H, 4-bromophenyl C_3), 7.55 (d, *J* = 5.4 Hz, 2H, phenyl C_3, C_5), 7.31 (d, *J* = 15.4 Hz, 1H, chalcone CH), 7.24 (t, *J* = 6.9 Hz, 2H, phenylpiperazine C_3, C_5), 7.03 – 6.78 (m, 5H, phenylpiperazine C_2, C_4, C_6, phenyl C_2, C_6), 3.46 (s, 4H, piperazine C_2,C_6), 3.30 (s, 4H, piperazine C_3,C_5). ^{13}C NMR (125 MHz, $CDCl_3$) δ 190.49 (C=O), 150.98 (4-bromophenyl C_1), 148.37 (4-bromophenyl C_2), 147.06 (4-bromophenyl C_6), 140.20 (chalcone CH), 134.07 (phenylpiperazine C_1), 130.71 (4-bromophenyl C_3,C_5), 129.79 (phenyl C_1), 129.29 (phenyl C_3, C_5, phenylpiperazine C_3, C_5), 126.68 (4-bromophenyl C_4), 124.84 (phenyl C_4), 123.14 (phenylpiperazine C_4), 120.36 (chalcone CH), 116.40 (phenylpiperazine C_2, C_6), 114.81 (phenyl C_2, C_6), 49.14 (piperazine C_2, C_6), 47.71 (piperazine C_3, C_5). MS (EI+):*m/z* calculated for $C_{25}H_{23}BrN_2O$: 447.38, found – 448.2310 (M+1), – 449.2311 (M+2).

(E)-1-(3-chlorophenyl)-3-(4-(4-phenylpiperazin-1-yl)phenyl)prop-2-en-1-one **(20)*:*** Yellow solid, yield: 82%, M.P.: 134-136°C. ^{1}H NMR (500 MHz, $CDCl_3$): δ 8.00 (s, 1H, 3-chlorophenyl C_2), 7.90 (d, *J* = 7.8 Hz, 1H, 3-chlorophenyl C_6), 7.82 (d, *J* = 15.6 Hz, 1H, chalcone CH), 7.62 (d, *J* = 8.7 Hz, 2H, phenylpiperazine C_3, C_5), 7.56 (d, *J* = 8.5 Hz, 1H, 3-chlorophenyl C_4), 7.47 (t, *J* = 7.9 Hz, 1H, 3-chlorophenyl C_5), 7.35 (d, *J* = 15.3 Hz, 3H, , phenyl C_3,C_5, chalcone CH), 7.09 – 6.89 (m, 5H, phenyl C_2,C_6, phenylpiperazine C_2, C_4, C_6), 3.52 (s, 4H, piperazine C_2,C_6), 3.38 (s, 4H, piperazine C_3,C_5). ^{13}C NMR (125 MHz, $CDCl_3$) δ 189.19 (C=O), 152.79 (3-chlorophenyl C_1), 151.01 (phenylpiperazine C_1), 145.96 (chalcone CH), 140.46 (3-chlorophenyl C_5), 134.80 (3-chlorophenyl C_3), 132.27 (3-chlorophenyl C_4), 130.41 (phenyl C_3, C_5), 129.86 (3-chlorophenyl C_2), 129.27

(phenylpiperazine C_3, C_5), 128.47 (3-chlorophenyl C_6), 126.43 (phenyl C_4), 125.28 (phenyl C_1), 120.33 (chalcone CH), 117.87 (phenylpiperazine C_4), 116.40 (phenylpiperazine C_2, C_6), 114.93 (phenyl C_2, C_6), 49.17(piperazine C_2, C_6), 47.86 (piperazine C_3, C_5). MS (EI+): *m/z* calculated for $C_{25}H_{23}ClN_2O$: 402.92, found – 403.4171 (M+1), 404.4153 (M+2).

(E)-1-(3-nitrophenyl)-3-(4-(4-phenylpiperazin-1-yl)phenyl)prop-2-en-1-one **(21)*:*** Dull yellow solid, yield: 83%, M.P.:135-137°C. ^{1}H NMR (500 MHz, $CDCl_3$): δ 7.80 (d, *J* = 7.9 Hz, 2H, 3-nitrophenyl C_4, C_6), 7.71 (d, *J* = 15.4 Hz, 1H, chalcone CH), 7.62 – 7.42 (m, 4H, phenyl C_2,C_6, phenylpiperazine C_3, C_5), 7.24 (q, *J* = 11.0 Hz, 3H, phenyl C_3,C_5, chalcone CH), 7.02 – 6.69 (m, 5H, phenyl C_2,C_6, phenylpiperazine C_2, C_4, C_6), 3.41 (s, 4H, piperazine C_2,C_6), 3.27 (s, 4H, piperazine C_3,C_5). ^{13}C NMR (125 MHz, $CDCl_3$) δ 189.43 (C=O), 152.74 (3-nitrophenyl C_3), 151.02 (phenylpiperazine C_1), 145.70 (chalcone CH), 137.54 (3-nitrophenyl C_1), 131.82 (3-nitrophenyl C_5, Phenyl C_1), 130.36 (3-nitrophenyl C_6, C_6), 129.96 (phenyl C_3, C_5), 129.29 (phenylpiperazine C_3, C_5), 127.40 (Phenyl C_4), 125.33 (3-nitrophenyl C_1), 120.33 (chalcone CH), 117.86 (phenylpiperazine C_4), 116.41 (phenylpiperazine C_2, C_6), 114.95 (phenyl C_2, C_6), 49.17 (piperazine C_2, C_6), 47.87 (piperazine C_3, C_5). MS (EI+): *m/z* calculated for $C_{25}H_{23}N_3O_3$: 413.48, found – 414.6124 (M+1).

(E)-3-(4-(4-(4-methoxyphenyl)piperazin-1-yl)phenyl)-1-phenylprop-2-en-1-one **(22)*:*** Pale yellow solid, Yield: 80%, M.P.:134-136 °C. ^{1}H NMR (500 MHz, $CDCl_3$) δ 7.85 (d, *J* = 8.1 Hz, 2H, phenylprop C_2, C_6), 7.52 (d, *J* = 15.23 Hz, 1H, chalcone CH), 7.50 – 7.43 (d, *J* = 8.4 Hz, 2H, phenyl C_3, C_5), 7.43 – 7.14 (m, 4H, phenylprop C_3, C_4, C_6, chalcone CH), 6.97 – 6.66 (m, 4H, phenyl C_2, C_6, 4-methoxyphenyl C_3, C_5), 6.66 – 6.54 (d, *J* = 7.9 Hz, 2H, 4-methoxyphenyl C_2, C_6), 3.86 (s, 3H, OCH_3), 3.68 (s, 4H, piperazine C_2,C_6), 3.54 (s, 4H, piperazine C_3,C_5). ^{13}C NMR (125 MHz, $CDCl_3$) δ 190.98 (C=O), 152.81 (4-

methoxyphenyl C_1), 149.85 (4-methoxyphenyl C_4), 144.36 (chalcone CH), 143.34 (phenylprop C_1), 138.27 (phenylprop C_4), 133.00 (), 131.73 (phenyl C_1), 129.07 (phenyl C_3, C_5) 128.34 (phenylprop C_3, C_5), 126.63 (phenylprop C_2, C_6), 122.95 (phenyl C_4), 121.43 (chalcone CH), 115.95 (4-methoxyphenyl C_3, C_5), 113.57 (4-methoxyphenyl C_2, C_6), 113.10 (phenyl C_2, C_6), 56.04 (OCH_3), 49.72 (piperazine C_2, C_6), 49.02 (piperazine C_3, C_5). MS (EI+): *m/z* calculated for $C_{26}H_{26}N_2O_2$: 398.51, found – 399.5603 (M+1).

***(E)-3-(4-(4-(4-methoxyphenyl)piperazin-1-yl)phenyl)-1-(p-tolyl)prop-2-en-1-one* (23):** Yellow solid, Yield: 72%, M.P.:133-135 °C. ^{1}H NMR (500 MHz, $CDCl_3$) δ 7.82 (d, *J* = 8.5 Hz, 2H, p-tolyl C_2, C_6), 7.49 (d, *J* = 15.31 Hz, 1H, chalcone CH), 7.32 – 7.13 (m, 5H, phenyl C_3, C_5, p-tolyl C_3, C_5, chalcone CH), 6.97 – 6.67 (m, 4H, phenyl C_3, C_5, 4-methoxyphenyl C_2, C_6), 6.54 (d, *J* = 8.4 Hz, 2H, 4-methoxyphenyl C_3, C_5), 3.86 (s, 4H, piperazine C_2,C_6), 3.67 (s, 4H, piperazine C_3,C_5), 2.39 (s, 3H, CH_3). ^{13}C NMR (125 MHz, $CDCl_3$) δ 190.98 (C=O), 152.81 (4-methoxyphenyl C_4), 146.85 (4-methoxyphenyl C_1), 144.36 (chalcone CH), 143.47 (p-tolyl C_4), 137.69 (p-tolyl C_1), 131.73 (phenyl C_1) 131.26 (p-tolyl C_3, C_5), 129.76 (p-tolyl C_2, C_6), 129.29 (phenyl C_3, C_5), 128.62 – 128.14 (m), 126.63 (phenyl C_4), 122.95 (chalcone CH), 115.95 (4-methoxyphenyl C_2, C_6), 113.57 (4-methoxyphenyl C_3, C_5), 111.10 (phenyl C_2, C_6), 56.04 (OCH_3), 49.65 (piperazine C_2, C_6), 47.61 (piperazine C_3, C_5), 21.13 (CH_3). MS (EI+): *m/z* calculated for $C_{27}H_{28}N_2O_2$: 412.53, found – 413.5311 (M+1).

***(E)-1-(3-bromophenyl)-3-(4-(4-(4-methoxyphenyl)piperazin-1-yl)phenyl)prop-2-en-1-one* (24):** Bright yellow solid, yield: 73%, M.P.: 138-140°C. ^{1}H NMR (500 MHz, $CDCl_3$) δ 7.97 (d, *J* = 15.6 Hz, 1H, chalcone CH), 7.69 (s, 1H, 3-bromophenyl C_2), 7.64 (m, 3H, phenyl C_3, C_5, 3-bromophenyl C_4), 7.38 – 7.21 (m, 3H, 3-bromophenyl C_5, C_6, chalcone CH), 6.86 (d, *J* = 8.2 Hz, 2H, phenyl C_2, C_6), 6.70 (d, *J* = 8.6 Hz, 2H, 4-methoxyphenyl C_2, C_6), 6.46 (d, *J* = 8.2 Hz, 2H, 4-methoxyphenyl C_3, C_5), 3.82 (s, 3H, OCH_3), 3.68 (s,

4H, piperazine C_2,C_6), 3.52 (s, 4H, piperazine C_3,C_5). ^{13}C NMR (125 MHz, $CDCl_3$) δ 190.71 (C=O), 152.81 (4-methoxyphenyl C_4), 149.85 (4-methoxyphenyl C_1), 144.36 (chalcone CH), 143.34 (3-bromophenyl C_2), 139.87 (3-bromophenyl C_1), 135.54 (3-bromophenyl C_4), 132.74 (phenyl C_4, 3-bromophenyl C_5), 131.44 (phenyl C_3, C_5), 130.52 (3-bromophenyl C_2), 127.08 (3-bromophenyl C_6), 126.63 (phenyl C_4), 123.43 (3-bromophenyl C_3), 122.95 (chalcone CH), 116.43 (4-methoxyphenyl C_2, C_6) 115.95 (4-methoxyphenyl C_3, C_5), 111.72 (phenyl C_2, C_6), 55.72 (OCH_3), 49.72 (piperazine C_2, C_6), 48.06 (piperazine C_3, C_5). MS (EI+): *m/z* calculated for $C_{26}H_{25}BrN_2O_2$: 477.40, found – 478.3581 (M+1), – 479.3533 (M+2).

***(E)-1-(4-bromophenyl)-3-(4-(4-(4-methoxyphenyl)piperazin-1-yl)phenyl)prop-2-en-1-one* (25):** Bright yellow solid, yield: 86%, M.P.: 133-135°C. ^{1}H NMR (500 MHz, $CDCl_3$) δ 8.19 (d, *J* = 15.2 Hz, 1H, chalcone CH), 7.94 (d, *J* = 8.2 Hz, 2H, 4-bromophenyl C_2, C_6), 7.65 (d, *J* = 8.6 Hz, 2H, 4-bromophenyl C_3, C_5), 7.51 - 7.35 (m, 3H, phenyl C_3, C_5, chalcone CH), 6.89 – 6.79 (m, 4H, 4-methoxyphenyl C_2, C_6, phenyl C_2, C_6), 6.50 (d, *J* = 8.2 Hz, 2H, 4-methoxyphenyl C_3, C_5), 3.85 (s, 3H, OCH_3), 3.65 (bs, 4H, piperazine C_2,C_6) 3.34 (bs, 4H, piperazine C_3,C_5). ^{13}C NMR (125 MHz, $CDCl_3$) δ 190.98 (C=O), 152.81 (4-methoxyphenyl C_4), 149.31 (4-methoxyphenyl C_1), 144.02 (chalcone CH), 140.28 (4-bromophenyl C_1), 132.36 (4-bromophenyl C_3, C_5), 131.88 (4-bromophenyl C_2, C_6), 131.26 (phenyl C_1), 129.93 (phenyl C_3, C_5), 128.38 (4-bromophenyl C_4), 125.32 (phenyl C_4), 123.25 (chalcone CH), 116.52 (4-methoxyphenyl C_2, C_6), 115.71 (4-methoxyphenyl C_3, C_5), 111.37 (phenyl C_2, C_6), 56.04 (OCH_3), 52.72 (piperazine C_2, C_6), 49.02 (piperazine C_3, C_5). MS (EI+): *m/z* calculated for $C_{26}H_{25}BrN_2O_2$: 477.40, found – 478.5310 (M+1), – 479.5361 (M+2)

(E)-1-(3-chlorophenyl)-3-(4-(4-(4-methoxyphenyl)piperazin-1-yl)phenyl)prop-2-en-1-one (26): Yellow solid, yield: 78%, M.P.: 133-135°C. ^{1}H NMR (500 MHz, $CDCl_3$)) δ

7.94 (s, 1H, 3-chlorophenyl C_2), 7.85 (d, *J* = 15.2 Hz, 1H, chalcone CH), 7.57 (d, *J* = 8.7 Hz, 2H, 3-chlorophenyl C_4, C_6), 7.47 – 7.28 (m, 3H, 3-chlorophenyl C_5, phenyl C_3, C_5), 6.88 – 6.79 (m, 3H, chalcone CH, phenyl C_2, C_6), 6.59 (d, *J* = 8.2 Hz, 2H, 4-methoxyphenyl C_2, C_6), 6.48 (d, *J* = 8.6 Hz, 2H, 4-methoxyphenyl C_3, C_5), 3.85 (bs, 4H, piperazine C_2,C_6), 3.53 (bs, 4H, piperazine C_3,C_5). ^{13}C NMR (125 MHz, $CDCl_3$) δ 190.71 (C=O), 152.76 (4-methoxyphenyl C_4), 149.85 (4-methoxyphenyl C_1), 144.36 (chalcone CH), 143.34 (3-chlorophenyl C_1), 140.56 (3-chlorophenyl C_3), 134.27 (3-chlorophenyl C_4), 132.33 (3-chlorophenyl C_5), 131.73 (phenyl C_1), 130.26 (3-chlorophenyl C_2), 129.91 (phenyl C_3, C_5), 126.53 (3-chlorophenyl C_6), 125.32 (phenyl C_4), 122.95 (chalcone CH), 116.43 (4-methoxyphenyl C_2, C_6), 115.53 (4-methoxyphenyl C_3, C_5), 112.10 (phenyl C_2, C_6), 56.31 (OCH_3), 51.43 (piperazine C_2, C_6), 48.71 (piperazine C_3, C_5). MS (EI+): *m/z* calculated for $C_{26}H_{25}ClN_2O_2$: 432.95, found – 433.71 (M+1), 434.7174 (M+2)

(E)-1-(4-chlorophenyl)-3-(4-(4-(4-methoxyphenyl)piperazin-1-yl)phenyl)prop-2-en-1-one (27): Yellow solid, yield: 82%, M.P.: 135-137°C. ^{1}H NMR (500 MHz, $CDCl_3$) δ 8.04 (d, *J* = 15.2 Hz, 1H, chalcone CH), 7.87 (d, *J* = 8.2 Hz, 2H, 4-chlorophenyl C_2, C_6), 7.61 (d, *J* = 8.6 Hz, 2H, 4-chlorophenyl C_3, C_5), 7.45 – 7.32 (m, 3H, phenyl C_3, C_5, chalcone CH), 6.74 – 6.63 (m, 4H, 4-methoxyphenyl C_2, C_6, phenyl C_2, C_6), 6.48 (d, *J* = 8.2 Hz, 2H, 4-methoxyphenyl C_3, C_5) 3.86 (s, 3H, OCH_3), 3.66 (bs, 4H, piperazine C_2,C_6), 3.32 (bs, 4H, piperazine C_3,C_5). ^{13}C NMR (125 MHz, $CDCl_3$) δ 190.96 (C=O), 152.27 (4-methoxyphenyl C_4), 149.85 (4-methoxyphenyl C_1), 144.36 (chalcone CH), 143.34 (4-chlorophenyl C_4), 138.69 (4-chlorophenyl C_3, C_5), 137.35 (4-chlorophenyl C_2, C_6), 131.73 (4-chlorophenyl C_1), 131.26 (phenyl C_1), 129.92 (phenyl C_3, C_5), 126.63 (phenyl C_4), 122.95 (chalcone CH), 116.43 (4-methoxyphenyl C_2, C_6), 115.57 (4-methoxyphenyl C_3, C_5), 111.10 (phenyl C_2, C_6), 56.32 (OCH_3), 51.74 (piperazine C_2, C_6), 49.41

(piperazine C_3, C_5). MS (EI+): *m/z* calculated for $C_{26}H_{25}ClN_2O_2$: 432.95, found – 433.7815 (M+1), 434.7824 (M+2).

(E)-1-(3-methoxyphenyl)-3-(4-(4-(4-methoxyphenyl)piperazin-1-yl)phenyl)prop-2-en-1-one (28): Bright yellow solid, yield: 78%, M.P.: 134-136°C. ^{1}H NMR (500 MHz, $CDCl_3$) δ 7.94 (d, *J* = 15.5 Hz, 1H, chalcone CH), 7.89 – 7.72 (m, 2H, chalcone CH, 3-methoxyphenyl C_5), 7.61- 7.48 (m, 4H, 3-methoxyphenyl C_6, phenyl C_3, C_5), 7.35 (s, 1H, 3-methoxyphenyl C_2), 7.12 (m, 3H, 3-methoxyphenyl C_4, phenyl C_2, C_6), 6.81 (d, *J* = 8.6 Hz, 2H, 4-methoxyphenyl C_2, C_6), 6.62 (d, *J* = 8.2 Hz, 2H, 4-methoxyphenyl C_3, C_5), 3.85 (s, 3H, OCH_3), 3.71 (s, 3H, OCH_3), 3.67 (bs, 4H, piperazine C_2,C_6), 3.55 (bs, 4H, piperazine C_3,C_5). ^{13}C NMR (125 MHz, $CDCl_3$) δ 190.71 (C=O), 159.93 (3-methoxyphenyl C_3), 152.81 (4-methoxyphenyl C_4), 149.85 (4-methoxyphenyl C_1), 144.36 (chalcone CH), 132.31 (3-methoxyphenyl C_6), 131.73 (3-methoxyphenyl C_1), 131.26 (phenyl C_1), 129.89 (phenyl C_3, C_5), 126.63 (s), 125.32 (phenyl C_4), 123.25 (chalcone CH), 116.31 (4-methoxyphenyl C_2, C_6), 115.73 (4-methoxyphenyl C_3, C_5), 114.32 (3-methoxyphenyl C_2, C_5), 111.42 (phenyl C_2, C_6),, 56.49 (OCH_3), 55.57 (OCH_3), 51.72 (piperazine C_2, C_6), 49.32 (piperazine C_3, C_5). MS (EI+): *m/z* calculated for $C_{27}H_{28}N_2O_3$: 428.53, found – 429.7121 (M+1).

(E)-3-(4-(4-benzylpiperazin-1-yl)phenyl)-1-phenylprop-2-en-1-one* (38)*: Yellow solid, Yield: 65%, M.P.: 169-171°C. ^{1}H NMR (500 MHz, $CDCl_3$) δ 8.03 (s, 1H, phenylprop C_4), 7.83 (d, *J* = 9.6 Hz, 1H, phenylprop C_2), 7.71 (d, *J* = 15.4 Hz, 1H, chalcone CH), 7.59 (d, *J* = 8.1 Hz, 1H, phenylprop C_6), 7.47 (d, *J* = 5.0 Hz, 2H, phenyl C_3, C_5), 7.26 (d, *J* = 14.0 Hz, 5H, phenylprop C_3, C_5, benzyl C3, C_4, C_5), 7.21 – 7.19 (m, 3H, chalcone CH, benzyl C_2, C_6), 6.80 (d, *J* = 8.1 Hz, 2H, phenyl C_2, C_6), 3.48 (s, 2H, (benzyl CH_2), 3.25 (bs, 4H, piperazine C_2,C_6), 2.51 (bs, 4H, piperazine C_3,C_5). ^{13}C NMR (125 MHz, $CDCl_3$) δ 189.06 (C=O), 152.99 (phenylprop C_3), 146.14 (chalcone CH), 140.73

(phenylprop C_5), 137.82 (phenylprop C_1), 135.14 (benzyl C_1, phenyl C_5), 131.38 (phenyl C_3, benzyl C_6), 130.42 (phenylprop C_4), 130.12 (phenyl C_1, benzyl C_2), 129.20 (phenylprop C_6), 128.36 (phenylprop C_2), 127.27 (benzyl C_5), 126.88 (benzyl C_3), 124.79 (benzyl C_4), 122.86 (chalcone CH), 117.48 (phenyl C_4), 114.64 (phenyl C_2, C_6), 63.04 (benzyl CH_2), 52.78 (piperazine C_2, C_6), 47.66 (piperazine C_3, C_5). MS (EI+): *m/z* calculated for $C_{26}H_{26}N_2O$: 382.51, found – 383.5871 (M+1). HPLC purity: 98.62%.

(E)-3-(4-(4-benzylpiperazin-1-yl)phenyl)-1-(p-tolyl)prop-2-en-1-one **(39):** Pale yellow solid, yield: 78%, M.P.:168-170 °C. ^{1}H NMR (500 MHz, $CDCl_3$) δ 7.94 (d, *J* = 7.9 Hz, 2H, p-tolyl C_2, C_6), 7.79 (d, *J* = 15.5 Hz, 1H, chalcone CH), 7.57 (d, *J* = 8.4 Hz, 2H, phenyl C_3, C_5), 7.44 - 7.36 (m, 5H, , benzyl C_3, C_4, C_5, p-tolyl C_3, C_5), 7.34 – 7.25 (m, 3H, chalcone CH, benzyl C_2, C_6), 6.91 (d, *J* = 8.5 Hz, 2H, phenyl C_2, C_6), 3.60 (s, 2H, benzyl CH_2), 3.34 (t, *J* = 5.1 Hz, 4H, piperazine C_2,C_6), 2.63 (t, *J* = 5.1 Hz, 4H, piperazine C_3,C_5), 2.45 (s, 3H, CH_3). ^{13}C NMR (125 MHz, $CDCl_3$) δ 190.19 (C=O), 152.74 (p-tolyl C_4), 144.78 (chalcone CH), 143.08 (p-tolyl C_1), 137.85 (benzyl C_1), 136.23 (phenyl C_1), 130.09 (phenyl C_3, C_5), 129.21 (p-tolyl C_2, C_6), 129.19 (p-tolyl C_3, C_5), 128.52 (benzyl C_2, C_6), 128.33 (benzyl C_3, C_5), 127.24 (benzyl C_4), 125.34 (phenyl C_4), 118.39 (chalcone CH), 114.78 (phenyl C_2, C_6), 63.04 (benzyl CH_2), 52.81 (piperazine C_2, C_6), 47.83 (piperazine C_3, C_5), 21.65 (CH_3). MS (EI+): *m/z* calculated for $C_{27}H_{28}N_2O$: 396.53, found – 397.6011 (M+1).

(E)-3-(4-(4-benzylpiperazin-1-yl)phenyl)-1-(3-bromophenyl)prop-2-en-1-one **(40):** Pale yellow solid, yield: 82%, M.P.: 170-172 °C. ^{1}H NMR (500 MHz, $CDCl_3$) δ 8.00 (dd, *J* = 8.0, 2.9 Hz, 2H, 3-bromophenyl C_2, C_4), 7.82 (s, 1H, 3-bromophenyl C_6),7.77 (d, *J* = 15.6, 2.9 Hz, 1H, chalcone CH), 7.54 (dd, *J* = 8.7, 2.9 Hz, 3H, 3-bromophenyl C_3, phenyl C_3, C_5), 7.49 (m, 2H, benzyl C_3, C_5), 7.40 – 7.24 (m, 4H, chalcone CH, benzyl C_2,C_4, C_6), 6.91 – 6.85 (d, *J* = 8.5 Hz, 2H, phenyl C_2, C_6), 3.57 (s, 2H, benzyl CH_2), 3.32 (s, 4H,

piperazine C_2,C_6), 2.60 (s, 4H, piperazine C_3,C_5). ^{13}C NMR (125 MHz, $CDCl_3$) δ 190.71 (C=O), 152.82 (3-bromophenyl C_1), 145.27 (chalcone CH), 138.86 (benzyl C_1), 137.84 (3-bromophenyl C_4), 132.35 (phenyl C_1, 3-bromophenyl C_2), 130.19 (phenyl C_3, C_5), 129.20 (benzyl C_2, C_6), 128.52 (benzyl C_3, C_5), 128.39 (benzyl C_4, 3-bromophenyl C_6), 128.35 (3-bromophenyl C_5), 127.26 (phenyl C_4), 125.17 (3-bromophenyl C_3), 118.33 (chalcone CH), 114.75 (phenyl C_2, C_6), 63.04 (benzyl CH_2), 52.80 (piperazine C_2, C_6), 47.77 (piperazine C_3, C_5). MS (EI+): *m/z* calculated for $C_{26}H_{25}BrN_2O$: 461.40, found – 462.2811 (M+1), 463.3802 (M+2).

(E)-3-(4-(4-benzylpiperazin-1-yl)phenyl)-1-(4-bromophenyl)prop-2-en-1-one **(41)*:*** Yellow solid, yield: 84%, M.P.: 168-170°C. ^{1}H NMR (500 MHz, $CDCl_3$) δ 7.92 – 7.86 (d, *J* = 8.5 Hz, 2H, 4-bromophenyl C_2, C_6), 7.79 (d, *J* = 15.5 Hz, 1H, chalcone CH), 7.67 – 7.62 (d, *J* = 8.4 Hz, 2H, 4-bromophenyl C_3, C_5), 7.57 (d, *J* = 8.6 Hz, 2H, phenyl C_3, C_5), 7.37 - 7.30 (m, 6H, chalcone CH, benzyl $C_{1,2,3,4,5}$), 6.91 (d, *J* = 8.6 Hz, 2H, phenyl C_2, C_6), 3.59 (s, 2H, benzyl CH_2), 3.39 – 3.32 (t, *J* = 5.1 Hz, 4H, piperazine C_2,C_6), 2.63 (t, *J* = 5.1 Hz, 4H, piperazine C_3,C_5). ^{13}C NMR (125 MHz, $CDCl_3$) δ 189.45 (C=O), 152.94 (4-bromophenyl C_4), 145.83 (chalcone CH), 137.82 (4-bromophenyl C_1), 137.60 (benzyl C_1), 131.79 (4-bromophenyl C_3, C_5), 130.32 (4-bromophenyl C_2, C_6), 129.93 (phenyl C_3, C_5), 129.19 (benzyl C_2, C_6), 128.35 (benzyl C_3, C_5), 127.31(phenyl C_1), 127.26 (benzyl C_4), 124.89 (phenyl C_4), 117.59 (chalcone CH), 114.67 (phenyl C_2, C_6), 63.03 (benzyl CH_2), 52.78 (piperazine C_2, C_6), 47.69 (piperazine C_3, C_5). MS (EI+): *m/z* calculated for $C_{26}H_{25}BrN_2O$: 461.40, found – 461.1220 (M), 462.1262 (M+1). HPLC purity: 99.74%.

(E)-3-(4-(4-benzylpiperazin-1-yl)phenyl)-1-(4-chlorophenyl)prop-2-en-1-one **(42)*:*** Yellow solid, yield: 75%, M.P.: 167-169°C. ^{1}H NMR (500 MHz, $CDCl_3$) δ 7.94 (dt, *J* = 8.5, 1.9 Hz, 2H, 4-chlorophenyl C_2, C_6), 7.77 (dt, *J* = 15.5, 2.1 Hz, 1H, chalcone CH),

7.54 (dt, *J* = 8.9, 1.8 Hz, 2H, 4-chlorophenyl C_3, C_5), 7.45 (dt, *J* = 8.6, 1.9 Hz, 2H, phenyl C_3, C_5), 7.37 – 7.31 (m, 4H, chalcone CH, benzyl C_2, C_4, C_6), 7.31 – 7.24 (m, 2H, benzyl C_3, C_5), 6.88 (dt, *J* = 9.0, 1.9 Hz, 2H, phenyl C_2, C_6), 3.58 – 3.55 (m, 2H, benzyl CH_2), 3.33 (dt, *J* = 6.5, 3.3 Hz, 4H, piperazine C_2,C_6), 2.60 (dt, *J* = 6.6, 3.4 Hz, 4H, piperazine C_3,C_5). ^{13}C NMR (125 MHz, $CDCl_3$) δ 189.27 (C=O), 152.91 (4-chlorophenyl C_4), 145.76 (chalcone CH), 138.67 (benzyl C_1), 137.16 (4-chlorophenyl C_1), 130.31 (4-chlorophenyl C_2, C_6), 129.80 (phenyl C_3, C_5), 129.22 (4-chlorophenyl C_3, C_5),128.81(benzyl C_2, C_6), 128.36 (benzyl C_3, C_5), 127.29 (phenyl C_1), 127.26 (benzyl C_4), 124.92 (phenyl C_4), 117.63 (chalcone CH), 114.69 (phenyl C_2, C_6), 63.02 (benzyl CH_2), 52.77 (piperazine C_2, C_6), 47.68 (piperazine C_3, C_5). MS (EI+): *m/z* calculated for $C_{26}H_{25}ClN_2O$: 416.95, found – 417.1727 (M+1), 418.1770 (M+2). HPLC purity: 99.81%.

(E)-3-(4-(4-benzylpiperazin-1-yl)phenyl)-1-(3-methoxyphenyl)prop-2-en-1-one **(43):** Bright yellow solid, yield: 73%, M.P.: 165-167°C. ^{1}H NMR (500 MHz, $CDCl_3$) δ 7.96 (s, *J* = 15.2 Hz, 1H, chalcone CH), 7.56 – 7.39 (m, 3H, 3-methoxyphenyl C_6, phenyl C_3, C_5), 7.39 – 7.24 (m, 7H, 3-methoxyphenyl C_2, C_5, benzyl $C_{2, 3, 4, 5, 6}$), 7.22 (s, *J* = 15.5 Hz, 1H, chalcone CH), 7.12 (bs, 1H, 3-methoxyphenyl C_4), 6.93 – 6.62 (m, 2H, phenyl C_2, C_6), 3.85 (s, 3H, OCH_3), 3.69 – 3.59 (m, 4H, piperazine C_2,C_6), 3.55 – 3.46 (m, 2H, benzyl CH_2), 2.85 – 2.76 (m, 4H, piperazine C_3,C_5). ^{13}C NMR (125 MHz, $CDCl_3$) δ 190.71 (C=O), 159.93 (3-methoxyphenyl C_3), 149.85 (chalcone CH), 144.36 (benzyl C_1), 138.23 (3-methoxyphenyl C_6), 131.73 (3-methoxyphenyl C_1), 130.29 (phenyl C_1), 129.04 (phenyl C_3, C_5), 128.40 (benzyl C_2, C_6), 126.59 (benzyl C_3, C_5), 122.95 (3-methoxyphenyl C_4), 121.45 (phenyl C_4), 119.42 (chalcone CH), 114.76 (3-methoxyphenyl C_2, C_5), 113.57 (phenyl C_2, C_6), 63.66 (benzyl CH_2), 56.04 (OCH_3), 51.02 (piperazine C_2, C_6), 48.72 (piperazine C_3, C_5). MS (EI+): *m/z* calculated for $C_{27}H_{28}N_2O_2$: 412.53, found – 413.3931 (M+1).

6.2.2 Prediction of ADMET properties

The ADME properties and toxicity predictions of all the synthesized compounds were calculated by the SwissADME (http://www.swissadme.ch/) and Biosigs's pkCSM web-server using SMILES strings of the compounds (http://biosig.unimelb.edu.au/pkcsm/prediction) (166, 180).

6.2.3 *In-vitro* cholinesterase inhibition assay

Previously reported protocols of modified Ellman colorimetric assay were used to assess the cholinesterase inhibitory activities of all the synthesized compounds (134, 181, 182). Briefly, the thiocholine was produced by the hydrolysis of thiolated substrates catalyzed by cholinesterase. It reduces the 5,5-dithio-bis-(2- nitrobenzoic acid) (DTNB) to give the yellow product that can be colorimetrically detected at **412** nm. The enzymes *ee*AChE (CAS No. 9001-08-1) and *eq*BuChE (CAS No. 9000-81-5) were purchased from Sigma Aldrich. Concisely, the stock concentrations of test compounds (**18-28** & **38-43**) were prepared in DMSO and further dilutions were made in PBS to determine the inhibitory potential of all the synthesized compounds. Briefly, the assay method involved, firstly, the incubation of enzyme, 50 µl of AChE (0.22 U/ml) or 50 µl of BuChE (0.06 U/ml) with 10 µl of the test or standard compound in 96-well plates at room temperature for 30 min. Further, 30 µl of the substrate, viz. ATCI (15 mM) or BTCI (15 mM) was added, and the solution was incubated for an additional 30 min. Finally, DTNB (1.5 mM) 160 µl solution was added to each well, and absorbance was measured at 412 nm using a 96-well microplate reader on Synergy HTX multi-mode reader (BioTek, USA). All components were included in the blank control except the enzyme. The assays were carried out in triplicate and experiments were repeated independently at least two-three times. The percentage inhibition for each of the test compounds was calculated using the

following equation: [(Ac − Ai)/Ac] × 100, where Ai is the absorbance in the presence of the inhibitors and Ac is the absorbance in the absence of the inhibitors.

6.2.4 *In-vitro* blood-brain barrier permeation assay

The *in vitro* brain permeability of the test compounds (**22-24**, **26** & **38-44**) was estimated by the PAMPA using an earlier reported protocol with minor modifications (183). Briefly, porcine brain lipid (20 mg/ml in dodecane) of 5 µl was coated on the bottom surface of porous filter disks of acceptor plates and was incubated overnight to get saturated. The stock solution of test compounds (10 mM) was prepared in DMSO of molecular biology grade, and further the dilution of 500 µM of 500 µl was made. The equilibrium standard of each test compound of 200 µl was made by dissolving 80 µl of 500 µM of test compounds with 120 µl PBS. Finally, the blank control of 250 µl was prepared by dissolving 5 µl of DMSO in 245 µl PBS buffer. The blank control and equilibrium standard were set aside for analysis on the next day. Then, 300 ul of PBS was filled in the acceptor plate. Each 500 µM of 200 µl test compound and permeability controls were added in duplicate to the wells of the donor plate (pore size of membrane 0.45 mm, Merck Millipore). The donor plate was carefully kept into the acceptor plate wells like a sandwich and incubated for 18 h at 37 ℃ to ease the diffusion of test molecules into the acceptor well from the donor part through lipid membrane. Donor plates were carefully removed on the completion of the incubation period, and absorbance of the drug in the acceptor, prepared equilibrium standard of each test compound and permeability and blank control were recorded using a microplate reader (HTX multi-mode reader, BioTek, USA). The absorbance of the test compound was mainly determined with recorded absorbance spectrum from wavelength of 200 nm to 500 nm in 10 nm intervals. The experiments were carried out in duplicate. The following expression was used to calculate the Pe value; $Pe = C \times -In\ (1- OD_A/OD_E)$ cm/s, where OD_A & OD_E

represent absorbance of acceptor and equilibrium standard respectively, and then C = 7.72×10^{-6}, if the experiment is running for 18 hrs. The results are given as the mean ± SD.

6.2.5 *h*BACE-1 inhibition assay

To estimate the BACE-1 inhibition activity of the synthesized lead molecules, a FRET-based fluorometric assay was carried out using the BACE-1 detection kit (CS0010, Sigma Aldrich, India) (184, 185). Briefly, the final volume of the assay solution contained 2 µl inhibitors (10 µM), 20 µl of substrate, and 78 µl fluorescent assay buffer. Then, 2 µl of *h*BACE-1 enzyme solution was added and the intensity of fluorescence was monitored at the respective excitation wavelength (λ_{ex} = 320 nm) and emission wavelengths (λ_{em} = 405 nm). The blank fluorescence intensity was subtracted from all the fluorescence signal readings. In the presence of the test compound, % inhibition was calculated by the following expression: [(IFo - IFi)/IFo] 100. Where, IFi and IFo represent the obtained fluorescence intensities with and without inhibitor, respectively.

6.2.6 Self-induced and AChE-induced $A\beta_{1-42}$ aggregation inhibition

$A\beta_{1-42}$ peptide was purchased from Cayman (India). The self as well as *ee*AChE-induced Aβ aggregation inhibition activities of the compound **41** were evaluated by thioflavin T assay (113). Firstly, the stock solution of 1 mg/ml of $A\beta_{1-42}$ was prepared by dissolving lyophilized aliquot of $A\beta_{1-42}$ in 80 µl of 1% NH_4OH and sterile PBS (920 µl, pH 7.4) and was stored at - 80 °C. Further dilutions were made with PBS solution to prepare a working solution of $A\beta_{1-42}$. For test compound **41**, the stock solution was made in DMSO and then final dilutions of 5 µM, 10 µM, and 20 µM were prepared with phosphate-buffered saline (PBS). Further, the concentration ratio of $A\beta_{1-42}$: test compound **41** (10:5, 10:10; and 10:20 µM) was evaluated (123, 186). In the assay of self-induced $A\beta_{1-42}$ aggregation inhibition, it contained $A\beta_{1-42}$ (10 µl; 10 µM) with PBS buffer (pH 7.4, 50 µM) and

incubated for 48 h at 37 ℃ in the presence or absence of compound **41** (10 µl; 5 µM, 10 µM, and 20 µM). Thioflavine T (178 µl, 20 µM) was added on the completion of the incubation time, and the fluorescence intensities were immediately measured at 450 nm and 405 nm. For the assay of *ee*AChE-induced $A\beta_{1-42}$ aggregation inhibition, the $A\beta_{1-42}$ (2 µl; 10 µM) and *ee*AChE (16 µl; 230 µM) was incubated at 37℃ for 48 h with or without compound **41** (2µl; 5 µM, 10 µM, and 20 µM). Thioflavin T (178 µl; 20 µM) was added after incubation time and intensities of fluorescence were measured (same as in self-induced). Blank readings were recorded with PBS with or without inhibitor instead of $A\beta_{1-42}$. The normalized fluorescence intensity (NFI) was recorded with respect to the control. All the experiments were carried out in triplicates and in three different independent runs.

6.2.7 Molecular docking

Molecular docking studies were performed to gain insight into the binding interaction of ligands with the protein. The molecular docking of compounds into the active sites of both AChE (4EY7) (187) and BACE-1 (2VKM) (188) was performed on Autodock 4 software. The protein structures were prepared in the Discovery Studio 2021 client version and structures of ligands were drawn on the Chem 3D. The grid parameters were fixed by considering amino acids from the AChE active sites and similarly for the BACE-1. The genetic algorithms selected were set to 100 runs. However, docking parameters were marked as default, followed by employing Lamarckian Genetic Algorithm (LGA). Further, the grid parameter file (gpf) and docking parameter file (dpf) were generated. Discovery studio visualizer software was used to visualized ligand–protein interaction (187).

6.2.8 Molecular dynamics

The Desmond module in the Schrodinger Maestro suite 2021 (academic version) with the OPLS 2005 force field was applied to perform the molecular dynamics simulation for the timescale of 100 ns. The molecular dynamics simulation of docked protein-ligand complexes of compound **41** with AChE/BACE-1 was performed. The open TIP3P (transferable intermolecular potential with 3 points) water model was used for the solvation of protein-ligand docked complexes in an orthorhombic core box of 10 Å radius (189). The steepest descent method minimized the complexes, followed by the BFGS (Broyden-Fletcher-Goldfarb-Shanno) algorithm. The studies were performed with the periodic boundary condition in the constant number of atoms, pressure, and temperature (NPT) ensemble. At a temperature of 300k and the atmospheric pressure of 1.013 bars relaxed using the default relaxation protocol. The complexes submitted to a production run of 100 ns, and a simulation run job was performed. The produced trajectories, Root mean square deviation (RMSD), Root means square fluctuation (RMSF), and protein-ligand interactions of the complexes were analyzed using depicted simulation interaction diagrams.

6.2.9 *In vivo* biological evaluations

6.2.9.1 Animals, housing, and ethical approval

Swiss albino mice of either sex were procured and kept for 7 days for acclimatization in the institute animal house facility (12:12 h dark/light cycle at 25 ± 2 °C) at the Department of Pharmaceutical Engineering & Technology, IIT(BHU). All the experimental protocols were approved (approval no. IIT(BHU/IAEC/2023/024) by the Institutional Animal Ethical Committee (IAEC), Indian Institute of Technology (BHU), Varanasi.

6.2.9.2 Acute oral toxicity studies

The acute oral toxicity tests were performed according to OECD 423 guidelines. The female albino mice were selected for the toxicity test. According to the guidelines, animals were divided into two groups (n = 3), group 1 was orally administered with vehicle alone (control group), and group 2 was administered with single dose of compound **41** (300 mg/kg, po). Mice were observed for 14 days for toxic symptoms, body weight, food consumption, behavioural changes, and mortality. Then, mice were sacrificed on the final day (after 14 days), and organs, i.e., brain, liver, kidney, and heart were collected. The tissue sections were made in transverse sections (15 µm) using a cryostat, mounted on the glass slide, stained with hematoxylin and eosin, and further observed on the microscope (Magnus MLX plus India at 10x resolution).

6.2.9.3 Behavioural studies (Scopolamine-induced amnesia model)

6.2.9.3.1 Drug preparation and treatment protocols

Scopolamine (3 mg/kg), DNZ (5 mg/kg), and compound **41** were freshly prepared in suspension (25, 50, and 100 mg/kg) of 0.3% sodium carboxy methyl cellulose. Animals were divided into six groups based on random selection (n = 6), including (i) Control, (ii) Scopolamine (3 mg/kg, i.p.), (iii) Compound **41** (25 mg/kg, p.o.), (iv) Compound **41** (50 mg/kg, p.o.), and (v) Compound **41** (100 mg/kg p.o.) (vi) DNZ, (5 mg/kg, p.o.). Test compounds and DNZ were administered daily for up to 7 days. On the seventh day the scopolamine (3 mg/kg, i.p.) was given to all groups excluding the control group after 30 minutes of drug administration. Only vehicles were given to the control group. After 15 minutes of the vehicle or scopolamine administration, all the animals were put through the Y-maze test.

6.2.9.3.2 Y-maze test

The widely used Y-maze test is a simple, quick, and sensitive test to assess spatial working and exploratory behavior in rodents (133). The spontaneous alternation score was examined with a three-dimensional horizontal maze set apart by 120°. Three different arms were named as A, B, and C. While testing, each mouse was placed at the center of three arms and allowed for free movement for 8 minutes. Each mice's entry into each arm was recorded using a video camera. Further, the obtained data was analyzed, and the percentage of alternation was calculated. The spontaneous alternation (SA) was considered when the mice entered successively into three different arms (ABC, ACB, BAC, BCA, CAB, and CBA). The percentage alternation was determined according to the formula: % spontaneous alternation (SA) = [(number of alternations/total arm entries) - 2] X 100. The % SA shows the short-term memory in mice (135).

6.2.9.4 *Ex-vivo* biochemical analysis

After completion of the behavioural experiment, all the mice were sacrificed immediately through the cervical dislocation. The brains were removed from the skull, and the hippocampus and cortex regions of the brain were isolated carefully, homogenized in 12.5 mM of 5 ml PBS (pH 7.4) with a glass homogenizer, and further supernatant were centrifuged at 7000 rpm for 30 min at 4°C. The supernatants were collected and used for the determination of various biochemical parameters. Primarily, the ACh levels were estimated using an acetylcholine ELISA kit (Krishgen Biosystems, India). The cholinergic marker, AChE was estimated using Ellman's colorimetric method with slight modifications (113, 134). In brief, the obtained supernatant (100 µl) was incubated for 5 min with the 15 mM of freshly prepared ATCI (100 µl), then added the 100 µl of DTNB (1.5 mM), and immediately the absorbance was recorded at 415 nm. CAT enzyme helps in the conversion of hydrogen peroxide into water and oxygen. The activity of CAT was

estimated as per the previously reported protocol. The assay mixture contained 50 µl of PBS (0.1 M; pH 7.4), 100 µl of dichromate/acetic acid solution (5% $k_2Cr_2O_7$/glacial acetic acid; 1:3 v/v), 50 µl of hydrogen peroxide (H_2O_2), and 50 µl of brain supernatant. Briefly, in the 96-well plate, 50 µl of supernatant, 50 µl of PBS, and 50 µl of 800 nM of hydrogen peroxide (H_2O_2) were incubated for 1 min at 37° C. Further, dichromate/acetic acid solution (150 µl) was added and boiled at 100° C for 10 min, and thereafter the absorbance was taken at 570 nm using a plate reader. The malondialdehyde (MDA), an oxidative stress biomarker of lipid peroxidation was measured using the thiobarbituric acid reactive substance (TBARS) assay. The assay protocol involved the mixing of 0.2 ml of 8.1% sodium lauryl sulphate, 1.5 ml of 0.8% aqueous thiobarbituric acid (TBA) solution, and 20% glacial acetic acid (1.5 ml) was added to the brain homogenate (0.2 ml). To the mixtures, deionized water was added up to 4.0 ml and heated for 60 min at 95 °C; further cooling was done with tap water, and n-butanol and pyridine mixture (15:1 v/v; 5 ml) and 1 ml of distilled water were added and centrifuged. The organic layer was separated and 200 µl of organic layer was added to a 96-well plate, and absorbance was taken at 532 nm using a microplate reader.

6.3 Results and discussions

6.3.1 Chemistry

The depicted **Scheme 6.1** was used to synthesize the designed compounds **18-28** and **38-43**. The reaction of 4-fluorobenzaldehye (**5**) with 1-phenylpiperazine (**6-7**) or benzylpiperazine (**30**) in the presence of a strong base potassium carbonate underwent nucleophilic substitution reaction to give intermediates (**8-9**) and **31,** respectively (190). The target compounds **(18-28)/ (38-43)** were synthesized by the reaction of obtained intermediate of substituted 1-phenylpiperazine/benzylpiperazine containing free aldehyde group with the substituted acetophenone (**10-17**)/(**32/37**). The reaction is base-

catalyzed condensation of acetone with aldehyde, where 2.5 M of NaOH solution is used as the base (191). It gives the alpha-beta unsaturated carbonyl compounds. The final substituted chalcone scaffolds containing phenylpiperazine **(18-28)** or benzylpiperazine **(38-43)** were obtained in good yield. All the synthesized scaffolds and intermediates were purified by column chromatography on silica gel (60–120 mesh) and characterized by ^{1}H (500 MHz), ^{13}C (125 MHz) NMR, and high-resolution mass spectrometry HRMS. The characterization spectra of the representative lead molecules are provided in the supporting information file. The % purity of the final compounds was assessed by HPLC analysis. The target compounds (**38**, **41** and **42**) were found to be > 98% pure (appendix).

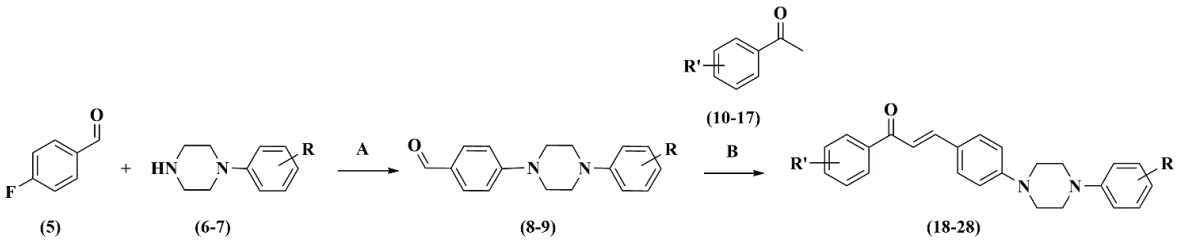

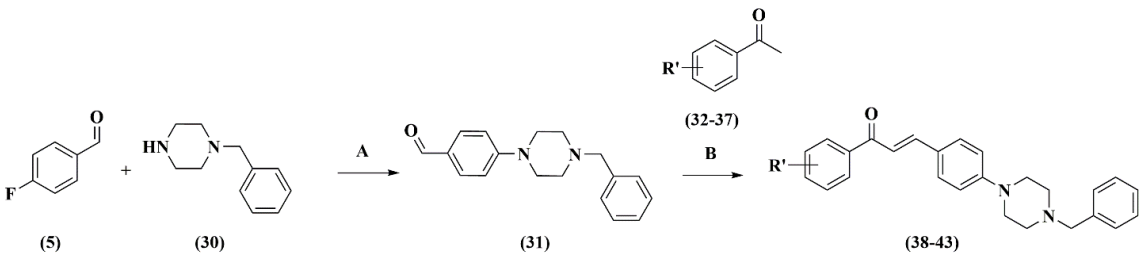

Scheme 6.1 [a] Reagents and conditions: (A) 4-Fluorobenzaldehyde (**5**)1.0 equiv, substituted 1-Phenylpiperazine (**6-7**)/ Benzylpiperazine (**30**) 1.0 equiv, Potassium carbonate 2.0 equiv, DMF,100^{o} C, 12 h; (B) Compound **8-9**/**31** 1.5 equiv, Substituted acetophenone (**10-17**/**32-37**) 1.0 equiv, 2 ml of 2.5 M NaOH Solution, Ethanol, rt, overnight.

6.3.2 Prediction of ADMET properties

The effective and safe drug should exhibit a finely tuned combination of pharmacodynamics and pharmacokinetic properties along with adequate absorption, distribution, metabolism, excretion, and tolerable toxicity (ADMET). ADMET properties of the molecules need to be considered in the drug discovery procedure for a better pharmacokinetic profile of the candidates (192). ADMET properties of all the synthesized molecules are depicted in **Table 6.1**. According to Lipinski's rule of five (RO5), orally bioavailable drug molecules should have less than 5 H-bond donors, 10 H-bond acceptors, molecular weight lower than 500, and MlogP value less than 4.15. The molecules violating more than one RO5 face difficulty in the absorption or permeation across a bio-membrane through passive diffusion (193). All the tested compounds were consistent with Lipinski's rule of five and did not show more than one violation. The lipophilicity parameter is an essential indicator of CNS permeation. The classical descriptor for lipophilicity is the partition coefficient between n-octanol and water (log Po/w). Interestingly, the log Po/w values of all the tested compounds were ranging from 3.21 to 4.65 (>3 & <5). The compounds containing one carbon linker, i.e., benzylpiperazine (**38-43**), showed comparatively higher lipophilicity than those without a carbon linker. The intestine is the primary site for the absorption of orally administered drugs. The proposition of compounds to be absorbed by the human small intestine is predicted. All the compounds showed more than 93 percent absorption through the human intestine. CNS permeability predictions are based on the blood-brain permeability-surface area product (logPS). The compounds with a more than -2 logPS are considered to penetrate the CNS. The lead compound **41** has been found to be the most permeable with the logPS of -0.791. However, all the compounds have logPS greater than > -2. The enzymes CYP2D6 and CYP3A4 participate in the metabolism of

DNZ. CYP2D6 enzyme mainly catalyzes the hydroxylation, deamination, and dealkylation. In contrast, the CYP3A4 enzyme catalyzes the oxidation of aldehydes, aromatic rings, and heteroatoms, along with olefinic epoxidation, hydroxylation, and N- and O-dealkylation (132). All the tested compounds **(18-28)/ (38-43)** were predicted to be a substrate for CYP3A4, and a few compounds were the substrate of CYP2D6. Drug-induced liver toxicity is the primary concern in drug development. The compounds were tested to predict the possibility of being associated with the disrupted normal function of the liver. Interestingly, the lead compound **41** has been found to be non-hepatotoxic.

Table 6.1: ADME and toxicity prediction of the compounds.

Comp	**Mol Wt (g/mol)**	**Lipinski violations**	**Log P o / w**	**Intestinal absorption**	**CNS permeability**	**CYP2D6 substrate**	**CYP3A4 substrate**	**CYP2D6 inhibitor**	**CYP3A4 inhibitor**	**Hepatotoxicity**
-	-	≤ 1	(>3 & <5	-	> -2	-	-	-	-	-
18	382.50	0	3.82	97.833	-0.984	No	Yes	No	Yes	No
19	447.37	1	3.95	96.308	-0.984	No	Yes	No	Yes	No
20	402.92	1	3.91	96.834	-0.994	No	Yes	No	Yes	No
21	413.47	0	3.21	96.564	-1.749	No	Yes	No	Yes	No
22	398.50	0	3.93	98.911	-1.086	No	Yes	No	Yes	Yes
23	412.52	0	4.06	98.882	-1.079	No	Yes	No	Yes	Yes
24	477.39	0	4.18	97.816	-1.089	No	Yes	No	Yes	Yes
25	477.39	0	4.16	97.357	-1.079	No	Yes	No	Yes	Yes
26	432.94	0	4.13	97.883	-1.089	No	Yes	No	Yes	Yes
27	432.94	0	4.02	97.424	-1.079	No	Yes	No	Yes	Yes
28	428.52	0	4.18	99.561	-1.176	No	Yes	No	Yes	Yes
38	382.50	0	3.96	95.091	-0.798	Yes	Yes	Yes	Yes	No
39	396.52	0	4.04	95.063	-0.791	Yes	Yes	Yes	Yes	No
40	461.39	1	4.19	93.996	-0.801	Yes	Yes	Yes	Yes	No
41	461.39	1	4.65	93.537	-0.791	Yes	Yes	Yes	Yes	No
42	416.94	1	4.04	93.604	-0.791	Yes	Yes	Yes	Yes	Yes
43	412.52	0	4.15	95.742	0.888	Yes	Yes	Yes	Yes	Yes
DPZ	379.5	0	3.92	93.707	-1.464	Yes	Yes	Yes	Yes	Yes

Note: The recommended compliance scores for all selected properties are provided in the final row for comparison with the reference values

6.3.3 *In-vitro* cholinesterase inhibition

The cholinesterase inhibitors can restore the depleted cholinergic function in AD by blocking the AChE enzyme that consequently increases the availability of ACh at the synaptic cleft. BuChE is an enzyme that could compensate for AChE in hydrolyzing central ACh. Therefore, dual inhibition of both AChE and BuChE is the appealing approach for the development of anti-AD agents (194). Accordingly, all the synthesized target compounds **(18-28)/ (38-43)** were evaluated for their inhibitory potential against *ee*AChE and *eq*BuChE. DNZ **(44)** and rivastigmine **(45)** were used as positive reference standards for *ee*AChE and *eq*BuChE evaluations, respectively. The obtained results of enzyme inhibition assays are summarized in **Table 6.2**. The chalcone scaffold was retained as a core nucleus in both series **(18-28) (38-43),** with modification at the piperazine ring. Among all the evaluated compounds, compounds **(38-43)** showed more pronounced inhibitory potential against AChE than the respective phenyl piperazine derivatives. The compounds containing one carbon linker, i.e., benzylpiperazine (**38-43**), showed better activities. Compound **41** bearing unsubstituted benzylpiperazine fragment and para-bromo substitution at chalcone scaffold exhibited potent inhibition of AChE ($\mathbf{IC_{50}}$, *ee*AChE (μM) = **14.84 ± 1.562**). The substitution of halogen at the chalcone scaffold of benzylpiperazine fragment-containing compounds (**38-43**) showed better activity. However, the position of the halogen substitution also affects the inhibition. The 4-substituted bromo analog showed superior activity than the corresponding 3-substituted. Further, the order of substituted halogen on *ee*AChE inhibition was Br > Cl for 4-halogen (195, 196). In the BuChE inhibition assay, **41** also turned out to be equipotent (% *eq*BuChE inhibition **41.39%±0.0164)** in comparison to other derivatives. The results indicated that the benzylpiperazine scaffold majorly contributed to the inhibitory activity. Conversely, compounds without carbon linker, i.e.,

phenyl piperazine, showed weak ChEs inhibition activity. However, compound **23**, containing phenylpiperazine, showed maximum inhibitory activities among all the derivatives **(18-28).** Another compound **22,** with a similar structure without substitution at the chalcone fragment, showed good inhibitory activities (AChE & BuChE). The substitution of the electron-donating group, -OCH_3, at the chalcone moiety diminished the AChE inhibitory potential in compounds **43, 28**. The strong electron-withdrawing substituted group, NO_2, in compound **21** did not improve the inhibitory activity. The inhibition of BuChE by compounds with one carbon linker, i.e., benzylpiperazine, was moderately higher compared to those without a carbon linker, i.e., phenylpiperazine.

6.3.4 *In-vitro* blood-brain barrier permeation assay

The blood-brain barrier (BBB) permeability of the molecules is the major concern for the development of drugs to treat AD. PAMPA-BBB was performed to explore the brain permeability of the selected synthesized compounds (183). The assay is widely used as an *in-vitro* model of passive transcellular permeation established based on the diffusion of molecules from the donor compartment to the acceptor well through the parallel artificial membrane. The reference permeability (Pe) values of 9 different commercial drugs were used as standard and Pe values were evaluated and reported in our previously published data (113). As per the threshold limit established by Di et al. for BBB permeation, Pe > 4.3×10^{-6} cm s^{-1} could cross the BBB (CNS+), 1.8×10^{-6} cm s^{-1} < 4.3×10^{-6} cm s^{-1} showed uncertain permeation through BBB (CNS ±), and Pe < 1.8×10^{-6} cm s^{-1} could not able to cross the BBB (CNS-). The obtained results (Pe values) of all tested compounds (**22, 23, 24, 26; 38-43**) are presented in **Table 6.2**. The tested compounds showed excellent ability as a BBB permeable (CNS+) and can reach their targets potentially within the brain. Compound **41** (Pe = **5.42 ± 0.275**) showed appreciable BBB permeability.

Table 6.2: Structures, cholinesterase inhibitory potential, PAMPA-BBB assay, and BACE1 inhibition of tested compounds.

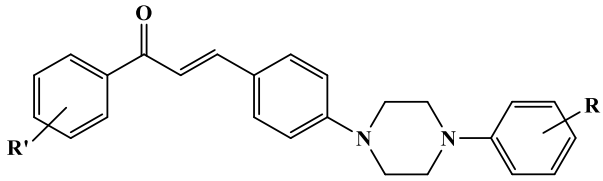

(18-28)

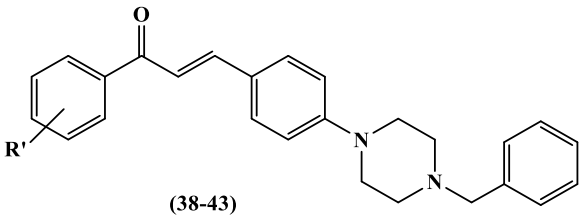

(38-43)

Com. No.	R	R'	IC_{50} (μM)[a] or % Inhibition[b]		Pe (10^{-6}cm s^{-1})	[c]BACE-1 % Inhibition
			*ee*AChE	*eq*BuChE		
18	H	4 - Methyl	28.75 ± 0.021%	n.a.	-	-
19	H	4 - Bromo	34.53 ± 0.030%	n.a.	-	-
20	H	3 - Chloro	45.04 ± 0.026%	28.00 ± 0.001%	-	-
21	H	3 - Nitro	31.03 ± 0.031%	n.a.	-	-
22	Methoxy	H	34.27 ± 1.859	26.77 ± 0.004%	7.56 ± 0.296	20.30 ± 1.90
23	Methoxy	4 - Methyl	30.41 ± 1.562	26.82 ± 0.002%	6.48 ± 0.197	33.54 ± 1.939
24	Methoxy	3 - Bromo	39.73 ± 0.045%	17.12 ± 0.002%	8.48 ± 0.282	-
25	Methoxy	4 - Bromo	46.44 ± 0.004%	24.66 ± 0.006%	-	-
26	Methoxy	3 - Chloro	31.97 ± 0.039%	13.96 ± 0.004%	6.48 ± 0.148	-
27	Methoxy	4 - Chloro	46.71 ± 0.008%	25.50 ± 0.012%	-	-
28	Methoxy	3 - Methoxy	35.81 ± 0.033%	28.06 ± 0.013%	-	-
38	-	H	29.63 ± 1.187	22.06 ± 0.003%	6.78 ± 0.268	43.66 ± 1.78
39	-	4 - Methyl	28.17 ± 0.601	19.80 ± 0.028%	7.97 ± 0.226	-
40	-	3 -Bromo	27.96 ± 0.268	30.58 ± 0.010%	5.44 ± 0.205	-
41	-	4 - Bromo	14.84 ± 1.562	41.39 ± 0.016%	5.42 ± 0.275	46.60 ± 1.748
42	-	4 - Chloro	19.4 ± 1.513	40.25 ± 0.021%	9.16 ± 0.240	45.851±1.306
43	-	3 - Methoxy	42.72 ± 0.026%	17.98 ± 0.002%	6.84 ± 0.403	-
44	DNZ	-	0.0656 ± 0.0049	-	9.36 ± 0.721	
45	Rivastigmine	-	-	1.23 ± 0.175	-	

[a]IC_{50}: 50% inhibitory concentration (mean ± SD of two or three independent experiments).

[b]% inhibition at 20 μM concentration of inhibitors.

[c]BACE-1 % Inhibition at 10 μM concentration of inhibitors. na not active.

6.3.5 *h*BACE-1 inhibition assay

To determine the BACE-1 inhibitory potential of selected synthesized compounds, the FRET-based fluorometric assay was performed (185). Compounds **22**, **23**, **38**, **41**, and **42**, with better anti-ChE activity, were evaluated for *in vitro h*BACE-1 inhibition to determine multi-targeting inhibitory potential (**Table 6.2**). Among all the evaluated compounds, compounds containing one carbon linker, i.e., benzylpiperazine **38, 41,** and **43**, showed significant activities at 10 μM of inhibitory concentration. However, compounds with phenylpiperazine scaffold exhibit moderate inhibition of *h*BACE-1. Compound **41**, bearing unsubstituted benzylpiperazine fragment and para-bromo substation at the chalcone scaffold, exhibited potent *h*BACE-1 inhibition. Based on overall *in vitro* findings, compound **41** was chosen as MTDLs for further investigation.

6.3.6 Self-induced and AChE-induced $A\beta_{1-42}$ aggregation inhibition

The major hallmark of AD is synaptic dysfunction and deposition of senile plaque, which are caused by the production, oligomerization, and self-aggregation of Aβ. The inhibition of Aβ aggregation has been considered as a potential and promising strategy in the search for effective AD therapy (197, 198). The anti-Aβ aggregation activity of lead compound **41** was evaluated with thioflavin T assay. Experiments were conducted for self and AChE-induced inhibition of $A\beta_{1-42}$ aggregation (**Figure 6.2**). It included three varied concentration ratios of the $A\beta_{1-42}$: compound **41** (10:5, 10:10, and 10:20 μM, respectively). DNZ was used as a reference, and the obtained results were depicted as normalized fluorescence intensity (NFI). The concentration-dependent inhibition of Aβ aggregation was observed in both the self and AChE-induced experiments. The maximal inhibitory potential was observed at 20 μM concentration of inhibitor (Aβ: Compound **41**, 10:20 μM). The obtained results demonstrated that compound **41** significantly inhibited the $A\beta_{1-42}$ aggregation activity in self- and AChE-induced experiments.

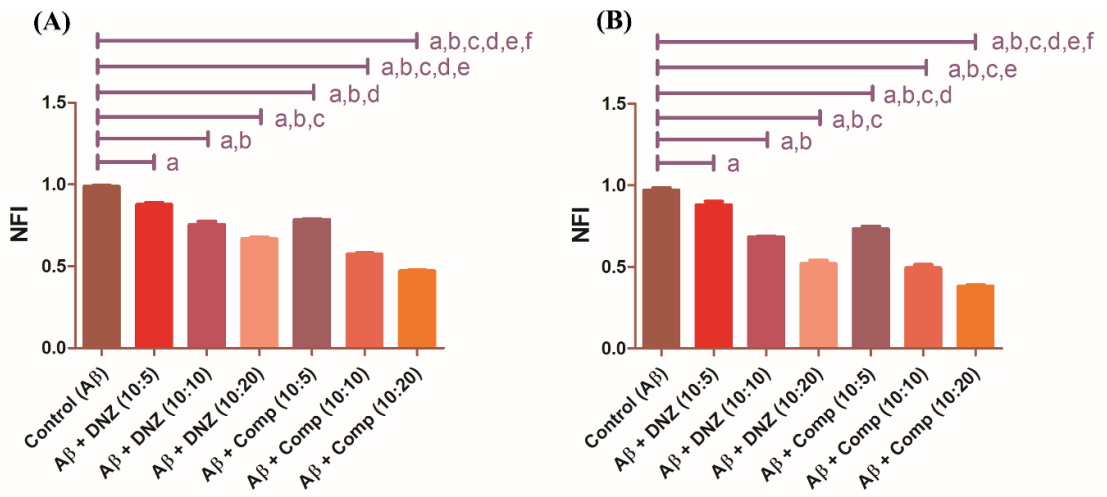

Figure 6.2. Effect of compound **41** on the $A\beta_{1-42}$ aggregation inhibition **(A)** Self-induced and; **(B)** AChE-induced. Bars are representing the NFI as the mean ± SEM of three independent experiments. $^{a}p< 0.05$ vs. Control (Aβ), $^{b}p < 0.05$ vs. Aβ + DNZ (10:5), $^{c}p < 0.05$ vs. Aβ + DNZ (10:10), $^{d}p < 0.05$ vs. Aβ + DNZ (10:20), $^{e}p < 0.05$ vs. Aβ + comp **41** (10:5), $^{f}p < 0.05$ vs. Aβ + comp **41** (10:10).

6.3.7 Molecular docking analysis

To gain insight into the binding interaction of compound **41** with the AChE (**4EY7**) and BACE-1 (**2VKM**) proteins, molecular docking studies were performed (199). The active sites of the AChE mainly consist of an esteratic site (Ser203, Glu334, and His447), anionic site (AS) (Trp86), and PAS, i.e., peripheral anionic site (Tyr72, Asp74, Tyr124, Trp286, and Tyr341) (132). The results of the molecular docking studies with AChE revealed that compound **41** interacted effectively with residues of the esteratic site, PAS, and the anionic site (**Figure 6.3).** The binding of prototype compound **41** showed that the para bromo phenyl ring located inside the CAS, i.e., the catalytic active site that formed π–alkyl interactions with amino acid, His447. The residue Trp86 formed the π–alkyl along with π–π stacked interactions with the para bromo phenyl ring, the principal residue of the anionic site. The principle chalcone scaffold of the molecules oriented towards the peripheral anionic site (PAS). The carbonyl group of the chalcone scaffold acted as a hydrogen bond acceptor and formed the hydrogen bonding interaction with Tyr341, an

essential residue of PAS along with Tyr337. Another PAS residue, Tyr124, participated by π–π stacked interactions. The residue Phe297 also formed π–π stacked interactions with the scaffold. Moreover, the benzyl piperazine moiety was found to form the π-interaction with Leu289 and Val294 and carbon-hydrogen bonding with the Ser293 residue. Additionally, interesting results were also obtained in the binding mode interaction of compound **41** with BACE-1 (**Figure 6.4**). The phenyl ring of the chalcone scaffold attached with piperazine displayed the π-anion bonding interaction with catalytic residue Asp228 of BACE-1 (200). The carbonyl group of the scaffold formed the strong hydrogen bonding interaction with Tyr198 residue. It was also involved in π–π stacked and carbon-hydrogen type interaction with flap region residues, Tyr71 and Thr72, respectively. Moreover, the *para* bromo phenyl ring is involved in the π–alkyl interaction with Val69 and Ile126 residue. The benzyl piperazine moiety makes the σ-π and π-donor interaction with Thr231 and Thr232, Gln73, and Gly230 residues, respectively.

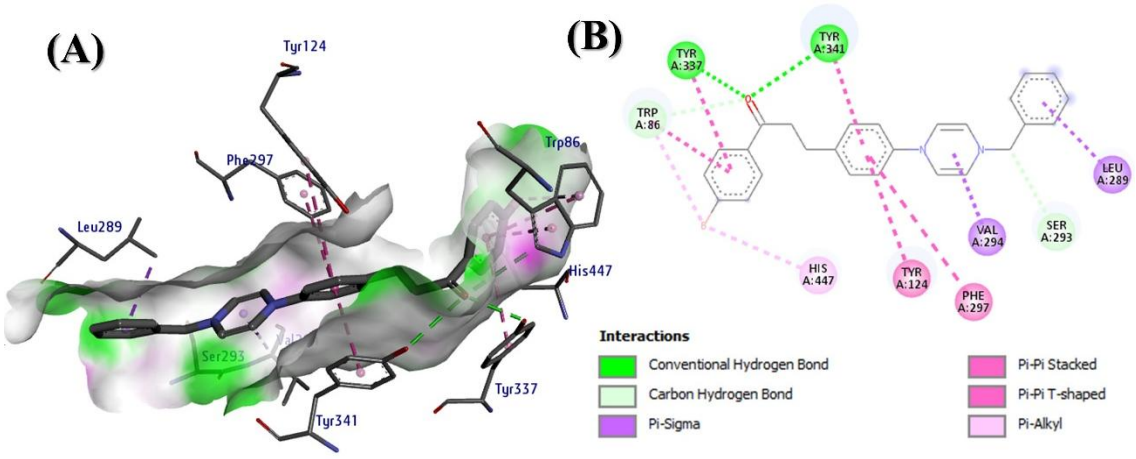

Figure 6.3 (A) 3D and (B) 2D binding interaction of compound **41** with AChE active site (PDB ID: 4EY7).

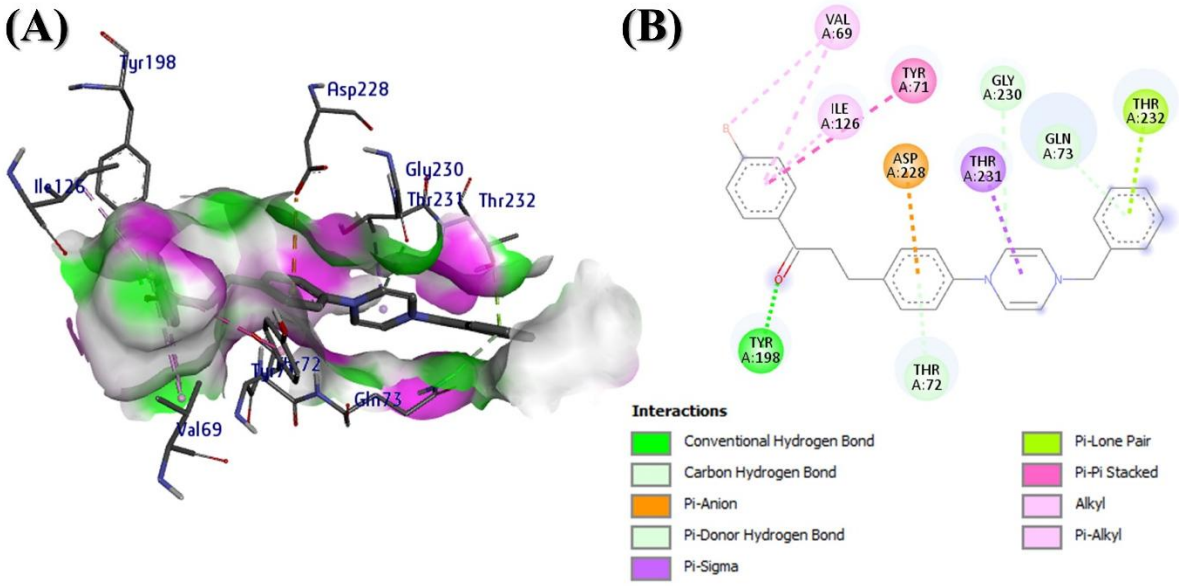

Figure 6.4 (A) 3D and (B) 2D binding interaction of compound **41** with BACE1 active site (PDB ID: 2VKM).

6.3.8 Molecular dynamics

The stability of docked complexes of compound **41** against both AChE and BACE-1 targets was affirmed with molecular dynamics simulation studies for the period of 100 ns. The simulation interaction diagrams were generated using trajectories, and the results were thoroughly analyzed. The RMSD of the protein backbone atoms and ligand were determined to measure the stability of the protein-ligand positions, relative to the protein backbone structure along with the RMSF. The ligand-protein RMSD of compound **41** with AChE was observed during the simulation (**Figure 6.5**). It showed the deviation at early 18 ns due to the early protein structural stabilization. Further, stable ligand RMSD was observed throughout the simulation period except for slight fluctuation at 40-43 ns and 70-75 ns. The sustained stability in RMSD of the protein backbone between 1.3 and 2.5 Å over the period of 100 ns was observed. The simulation analysis indicated that the binding of compound **41**-AChE at the CAS region was stable and interacted with the important amino acid His447. The PAS residues, including Asp74, Tyr124, Trp286, and Tyr341, effectively interacted with compound **41** through

hydrophobic or charged interaction. The stability of the binding interaction of compound **41** within the active site of BACE-1 was analyzed (**Figure 6.6**). The gradual and stable increase in the protein RMSD within the range of 0.9 to 2.8 Å was observed with minimal fluctuation. The complex stabilized early at 18 ns. Then, the steadiest and most stable RMSD of ligand was stretched out between 1.5 to 7.5 Å with the major fluctuation around 90 ns. The interaction of catalytic residue Asp228 of BACE-1 with compound **41** was displayed during the simulation. Another essential residue, Asp32, was involved in interaction with **41** by ionic interaction throughout the simulation period. Moreover, additional interaction with amino acid residues such as Tyr71, Thr72, Trp115, Tyr 198, and Lys224 showed that the results were in accordance with docking studies and the stabilization of **41**-BACE-1. Thereby, molecular dynamics simulation results indicated the potential of compound **41** against both AChE and BACE-1 targets.

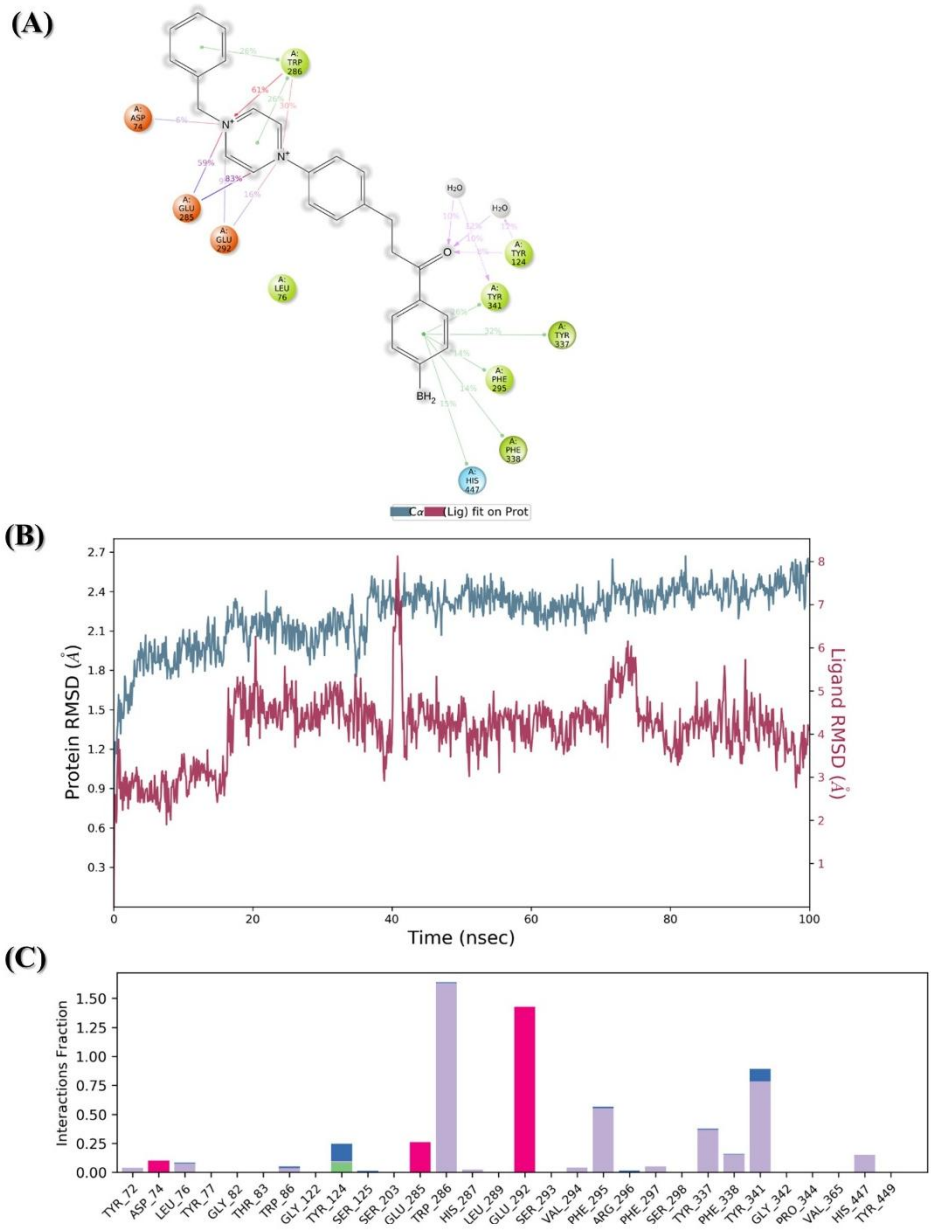

Figure 6.5. Analysis of molecular dynamics studies of compound **41**-AChE (4EY7) docked complex (**A**) graphical representation showing percentage interaction (**B**) RMSD plot of complex during 100-ns simulation runs (**C**) Histogram showing interaction fractions with active amino acid residue.

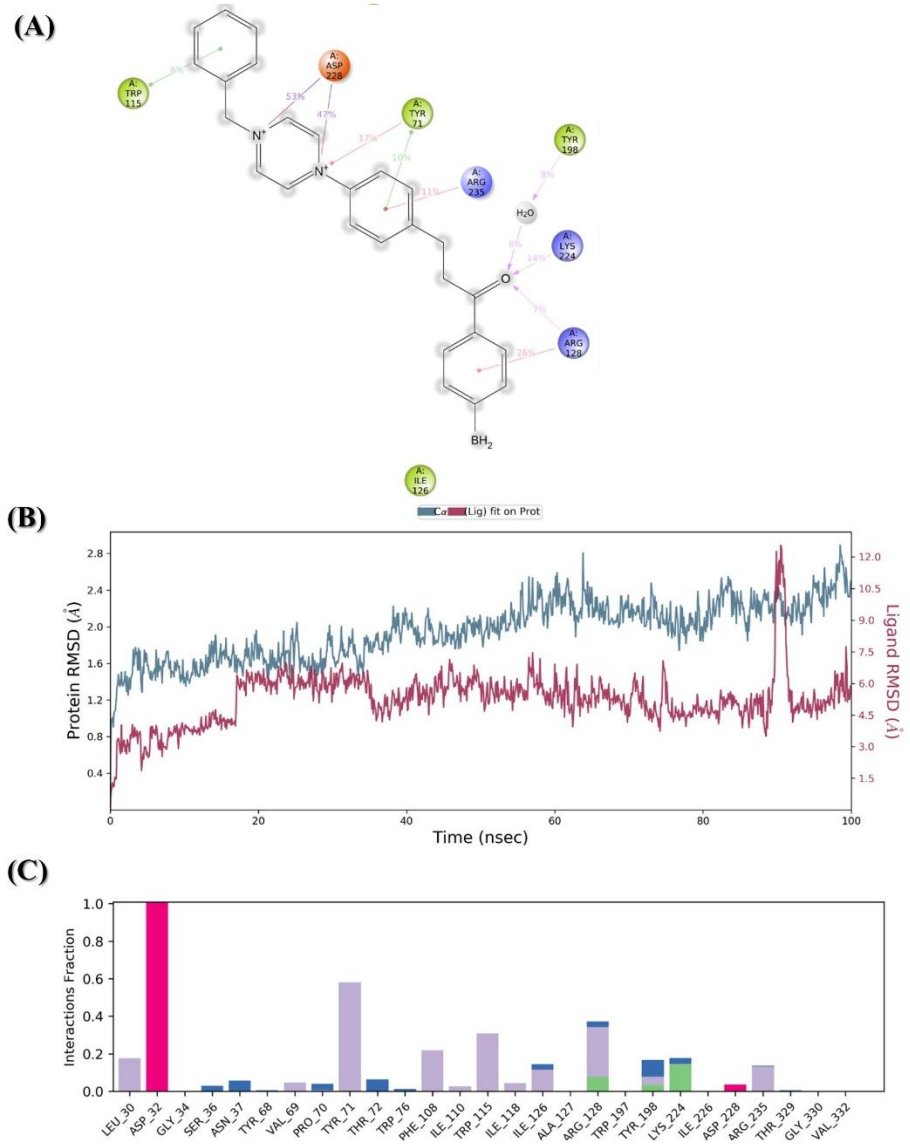

Figure 6.6. Analysis of molecular dynamics studies of compound **41**-BACE-1 (2VKM) docked complex (**A**) graphical representation showing percentage interaction (**B**) RMSD plot of complex during 100-ns simulation runs (**C**) Histogram showing interaction fractions with active amino acid residue.

6.3.9 *In vivo* biological evaluations

6.3.9.1 Acute oral toxicity studies

The safety profile of lead compound **41** was assessed with acute oral toxicity as per the OECD guideline 423 in female mice. The results demonstrated the absence of toxic effects i.e., behavior, body weight or changes in food and water intake, mortality after

administration of compound **41**. There was no notable histological damage found in the brain, liver, heart, or kidneys at a dose of up to 300 mg/kg **(Figure 6.7)**.

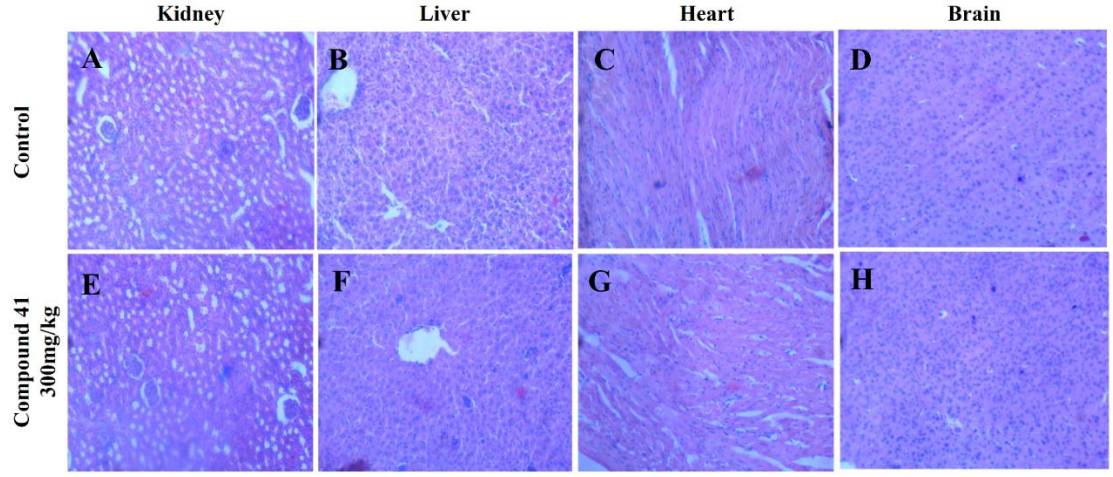

Figure 6.7. Effect of compound **41** on organ toxicity. (**A–D**) indicates histological abnormalities in kidney, liver, heart, and brain, respectively in the control group without treatment. (**E–H**) indicates the effect of compound **41** on histological abnormalities in kidney, liver, heart, and brain, respectively.

6.3.9.2 Behavioural studies

The behavioural studies were performed to evaluate the *in vivo* efficacy of compound **41** to ameliorate cognitive dysfunction and memory improvement in the scopolamine-induced cognitive deficit mouse model (123). The alternation in the scopolamine-induced memory impairment along with the treatment of compound **41**, was assessed with the Y-maze test (151, 152). The spontaneous alternation behavior activity of compound **41** (25, 50, and 100 mg/kg) along with the DNZ (5 mg/kg) was determined (**Figure 6.8**). The sequential arm entries and % spontaneous alternation score was measured along with the total arm entries of respective animals. One-way Annona revealed significant differences among all the groups. The percentage alternation was decreased ($p < 0.05$) in the scopolamine-treated mice, as compared to the control mice. A significant increase in the % spontaneous alternation was observed in the compound **41** treated group. Further, statistically significant difference was found in the group treated with compound **41** at a

dose of 25 mg/kg in spontaneous alternation as compared to 50 mg/kg and 100 mg/kg of dose. On the other hand, compound **41** at doses of 50 mg/kg and 100 mg/kg group did not show any significant difference ($p > 0.05$) in comparison to DNZ-treated mice. The findings revealed that administration of compound **41** produced significant improvement in cognitive and memory function in the scopolamine-induced mice model.

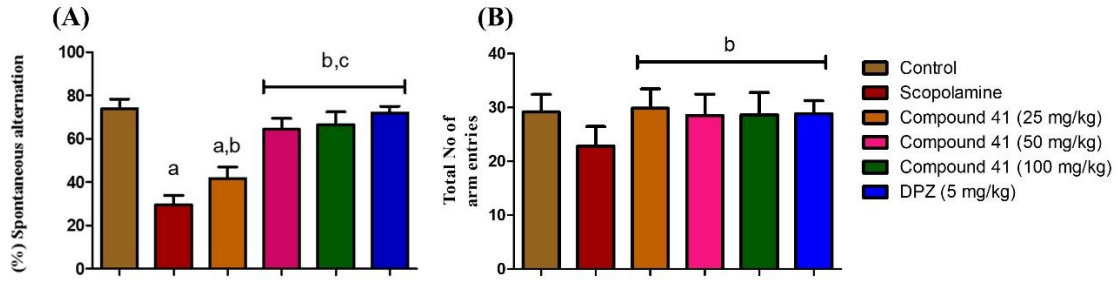

Figure 6.8. Effect of compound **41** on scopolamine induced cognition and memory impairment. (**A**) Effect of compound **41** on % spontaneous alternation. (**B**) Total no of arm entries. $^{a}P < 0.05$ vs. control; $^{b}P < 0.05$ vs. scopolamine; $^{c}P < 0.05$ vs. compound **41** (25 mg/kg). One-way ANOVA followed by Newman - Keuls posthoc test.

6.3.9.3 *Ex-vivo* biochemical analysis

The potential effects of compound **41** at the neurochemical levels were established by estimating the ACh and AChE levels along with other biochemical parameters such as malondialdehyde (MDA) and catalase (CAT). Immediately after the completion of behavioural studies, the mice of the respective groups were decapitated and the hippocampus region of the brain was isolated and homogenized. The *ex vivo* estimation of ACh was performed using an ELISA kit and AChE was assessed with the Ellman assay (134). The results demonstrated that the ACh levels were decreased and AChE activity was increased in the scopolamine-treated mice as compared to the control group ($p < 0.05$). However, compound **41** treated group showed an increase in the ACh levels significantly and a decrease in the AChE levels compared to scopolamine-treated mice ($p < 0.05$). Further, the antioxidant properties of compound **41** were annotated by the determination of oxidative biochemical markers such as MDA and CAT. The results

revealed that the scopolamine-treated mice significantly decreased CAT levels and elevated the MDA levels as compared to the control group ($p < 0.05$) (**Figure 6.9**). However, the treatment with compound **41** attenuated the levels of MDA while remarkably increasing the levels of CAT compared to scopolamine-treated mice. The results also showed that the CAT levels increased and MDA decreased significantly in the DNZ-treated group ($p < 0.05$). Thus, collectively the obtained results of *ex vivo* biochemical analysis suggested AChE inhibitory potential of compound **41** along with antioxidant property.

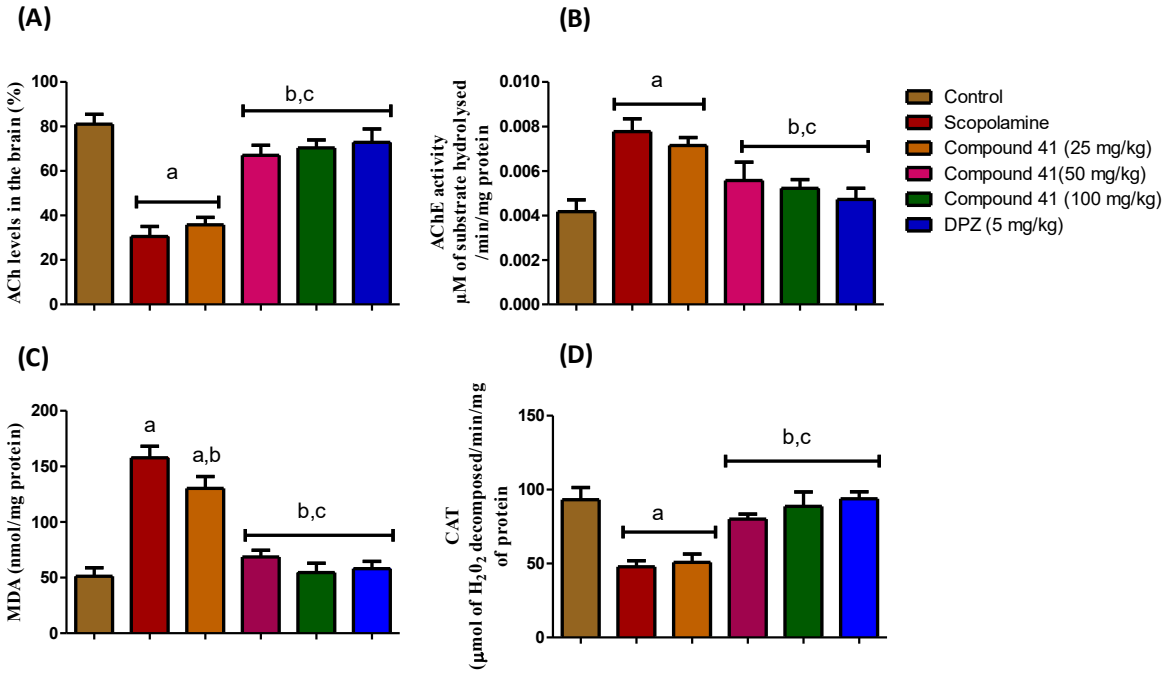

Figure 6.9. Effect of compound **41** on *ex vivo* biochemical parameters. (A) Effect of compound **41** on ACh levels. (B) AChE activity, (C) MDA level and (D) CAT activity. $^{a}P < 0.05$ vs. control; $^{b}P < 0.05$ vs. scopolamine; $^{c}P < 0.05$ vs. compound **41** (25 mg/kg). One-way ANOVA followed by Newman - Keuls posthoc test.

6.4 Summary and conclusion

The multi-factorial nature of AD, comprising the presence of $A\beta_{1-42}$ aggregation, lower level of ACh, along with neurotoxicity created an urgent need to explore multi-targeted therapeutics to treat the disease. A scaffold hopping-guided MTDLs strategy was

delineated in the present study for the design of multifunctional molecules for the treatment of AD. A series of substituted chalcone scaffolds containing phenylpiperazine or benzylpiperazine derivatives **(18-28) (38-43)** were synthesized and evaluated for their multi-targeting ability. The synthesized compounds were initially investigated *in vitro* ChEs (*ee*AChE and *eq*BuChE) inhibitions. In comparison to all the tested derivatives, compounds **22**, **23**, **38**, **41** and **42** with potential anti-cholinesterase activity were further evaluated for *h*BACE-1 inhibition. Compound **41** bearing unsubstituted benzylpiperazine fragment and para-bromo substation at chalcone scaffold exhibited potent AChE inhibitory activity, IC_{50} = **14.84 ± 1.562 µM** and significant BuChE inhibition. The compound also produced a remarkable influence on the *h*BACE-1 inhibitory potential as compared to other compounds from the series. The notable inhibition of $A\beta_{1-42}$ aggregation with maximal inhibitory potential at 20 µM inhibitor concentration was observed in both self- and AChE-induced assay, which indicated the multi-targeting potential of compound **41**. Based on the findings, it may be inferred that the presence of a carbon linker joining the piperazine and aryl ring-bearing electronegative substituent at the para position improved activity. The *in silico* ADMET, molecular properties analyses and BBB permeability were also determined. Furthermore, compound **41**, evaluated on the scopolamine-induced amnesia model, produced a significant reversal of learning and memory functions at 50 mg/kg of dose. The *ex-vivo* biochemical analysis indicated a comparable reduction in AChE and an increase in ACh levels. The antioxidant potential of compound **41** was evaluated with the assessment of levels of oxidative biochemical markers such as MDA and CAT. The treatment of compound **41** attenuated the levels of MDA and CAT significantly. Overall, the findings indicated compound **41** to be the most promising multi-target directed ligand and a promising "lead" for the treatment of AD.